SUB-BASALT IMAGING: MODELING AND DEMULTIPLE

A Thesis

by

SHANTANU KUMAR SINGH

Submitted to the Office of Graduate Studies of
Texas A&M University
in partial fulfillment of the requirements for the degree of

MASTER OF SCIENCE

December 2005

Major Subject: Geophysics

SUB-BASALT IMAGING: MODELING AND DEMULTIPLE

A Thesis

by

SHANTANU KUMAR SINGH

Submitted to the Office of Graduate Studies of
Texas A&M University
in partial fulfillment of the requirements for the degree of

MASTER OF SCIENCE

Approved by:	
Chair of Committee,	Luc T. Ikelle
Committee Members,	Hongbin Zhan
	Thomas A. Blasingame
Department Head,	Richard L. Carlson

December 2005

Major Subject: Geophysics

ABSTRACT

Sub-Basalt Imaging: Modeling and Demultiple. (December 2005)

Shantanu Kumar Singh, B.Sc., Lucknow University;

M.Tech, University of Roorkee, India

Chair of Advisory Committee: Dr. Luc T. Ikelle

Seismic imaging of sub-basalt sedimentary layers is difficult due to high impedance of the basalt layer, the roughness of the top and bottom of the basalt layer and sometimes the heterogeneities within the basalt layer. In this thesis we identify specific problems within the modern imaging technology which limit sub-basalt imaging. The basic framework for the identification of this limitation is that we are able to group most basalt layers into the following four categories:

- A basalt layer having smooth top and bottom surfaces.
- A basalt layer having rough top and bottom surfaces.
- Small-scale heterogeneities within the basalt layer.
- Intra-basalt velocity variation due to different basalt flows.

All the above models of basalt layers obviously have high impedance with respect to the surrounding sedimentary layers. These four models encapsulate all the possible heterogeneities of basalt layers seen in areas like the Voring and More basins off mid-Norway, basins in the Faroes, W. Greenland, Angola and Brazil margins, and the Deccan Traps of India.

In this work, problems in seismic processing and imaging specific to these models have been presented. For instance, we have found that the application of the multiple attenuation technique, which first predicts the multiples and then subtracts them from the data, using least-squares criteria, can be effective for all the models except for the model, which has intra-bedded layers within the basalt. The failure in the second case is due to the destructive interference of multiple scattering from the intra-bedded layers within the basalt and the multiples located below the primary associated with the top of the basalt layer. This interference degrades the signal-to-noise (S/N) ratio of the multiples contained in the data, whereas the predicted multiples, which are constructed from the reflectors above the basalt, have a much higher signal-to-noise ratio. Our recommendation is to subtract the predicted multiples from the data using either least-absolute-value criteria or any other higher-order-statistics-based criteria.

DEDICATION

To my wife and beloved daughters

ACKNOWLEDGMENTS

I would like to take the opportunity to sincerely thank my academic advisor and chair, Dr. Luc T. Ikelle, for his timely guidance and support that have been fundamental to my growth as a professional geophysicist. In particular I would like to thank him for helping me define my goal and for providing insight into the research problem. His availability and his willingness to spend his valuable time in guiding me through my problems is something that that I will always be grateful for.

I would also like to express my gratitude to my committee members, Dr. Hongbin Zhan and Dr. Thomas A. Blasingame, for their comments and valuable time. I would also like to thank Dr. Daulat Mamora for agreeing to help.

I express my special thanks to all the CASP members for their valuable time and suggestions without which I may not have been able to complete the thesis on time. I would take the opportunity to thank the CASP project also for providing me with all the resources required to achieve my goal.

Last, but most importantly, I would like to thank my wife Ritu for supporting me throughout my study.

TABLE OF CONTENTS

CHAPTER Page

LIST OF TABLES

LIST OF FIGURES

FIGURE Page

FIGURE Page

FIGURE Page

FIGURE Page

CHAPTER I

INTRODUCTION

Imaging of sub-basalt layers in areas like the Voring and More basins off mid-Norway, basins in the Faroes, West Greenland, Angola, and Namibia basins; the Brazil margins, the Western Australian basins; and the Deccan Traps of India (see Figure 1.1) is very important today, as these basaltic basins are known to be potential hydrocarbon reservoirs. The basalts that have intruded the sedimentary rocks are known to have increased maturation of sub-basalt source rocks due to increased burial.

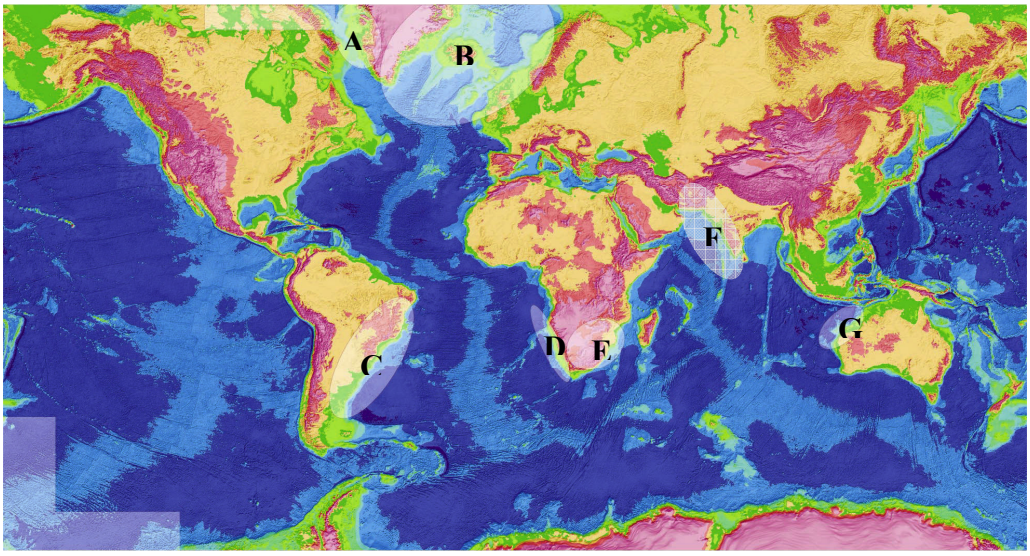

Figure 1.1: Important hydrocarbon deposits related to volcanic complexes. A=W. Greenland basins, B=Voring and More basins and Faroes basins, C=Brazil and Argentina basins, D=Angola and Namibia basins, E= Karoo basins, F=Deccan Traps and G=NW Australian basins.

This thesis follows the style and format of Geophysics.

They also influence the migration pathways of hydrocarbons due to the deposition of low permeability basalt flows that acts as a very good cap rock/seal.

BACKGROUND OF SUB-BASALT TRAPS

Let me expand on the basalt basins and their importance in the context of hydrocarbon reservoirs. For many years it has been known that volcanic basins can be potential hydrocarbon reservoirs due to the following properties.

- Regional environmental changes caused by the release of volatiles and particles into the atmosphere, influencing the paleoclimate and possibly leading to mass extinction.
- Increased maturation of sub-basalt source rocks due to increased burial and proximity to high-temperature volcanic deposits.
- Change in migration pathways due to the position of low-permeability basalt flows that act as seals.

Due to extensive volcanism, large volumes of volatiles released into the atmosphere may have brought some drastic change in the paleoclimate that led to the mass extinction of organisms. These dead organisms would then have become a good source of hydrocarbons in an anoxic environment, which is essential for the formation of hydrocarbons. Also, an increase in temperature in the neighborhood of volcanic flows and the burying of these organic-rich sediments under a thick basalt layer may have led to increased maturation of hydrocarbons. These basalts not only helped in maturation but

also acted as a good seal, thus affecting the migration of the hydrocarbons by restricting their movement and accumulating them in structural highs below them, leading to hydrocarbon trap formation.

CHALLENGES OF SUB-BASALT IMAGING AND PAST CONTRIBUTIONS

Despite all this knowledge, very little work has been done on the imaging of volcanic basins. Imaging of sub-basalt horizons is very difficult because of the complex behavior of basalt and the inability of conventional acquisition and processing techniques to attenuate the noise that obscures the sub-basalt reflections. Due to the high velocity and density of the basalt with respect to the surrounding sedimentary layers, very little energy passes through the basalt layer, making the underlying reflections very weak and difficult to image. In addition, the rough basalt top and bottom scatter the energy, and small-scale heterogeneities within the basalt produce significant multiple scattering that totally obscure the weak sub-basalt reflections.

The moving of exploration and production (E&P) to deep waters, combined with recent advances in seismic acquisition and imaging technology, E&P of sub-basalt hydrocarbon reservoirs, is becoming more and more feasible. Ocean-bottom seismics (OBS) is one such example of acquisition technique, which provides us more shear-wave (S-wave) information in addition to primary-wave (P-wave) information.

Improvements in seismic imaging, including accurate velocity model building, decomposition of data into P-waves and S-waves, pre-stack depth migration, and multiple attenuation, which increases the resolution of data and imaging of the sub-basalt hydrocarbon reservoir, has become a reality. Intelligent data processing based on an understanding of the behavior of basalt can help in choosing the right parameters to reduce the noise and bringing up the weak reflections, as discussed in this thesis.

New acquisition and processing methods have been proposed to overcome the problem of sub-basalt imaging. Recent works on sub-basalt imaging are very well captured in a special issue of *Geophysical Prospecting*, 2003. All the papers in this issue are included in the references list of this thesis. We will be discussing some of these papers and then in the next section highlight their shortcomings. For example, Ziolkowski et al. (2003) proposed using of a low-frequency source. The advantage of using a low-frequency source, as shown in this paper, is that the lower the frequency less is the scattering of energy from the rough top and bottom of the basalt. This will help in recording stronger events from the sub-basalt horizons and less noise due to scattering. A large number of papers in this issue discussed the importance of wide-angle/large-aperture multicomponent OBS acquisition for basalt models. These studies are based on the fact that the wide-angle reflection data (with super long receiver arrays ~38 km maximum offset) will help in getting higher amplitudes at near-critical angles. Multiples created in sedimentary layers above the basalt will be absent at wide-angles, and travel-time data from wide-angle refraction arrivals allow an improved migration-velocity model to be constructed. Barton and Barker (2003), proposed an automated method for

generating the velocity fields from travel time picked on refracted data. These picks are transformed into the τ-p domain from both source and receiver gathers and the apparent velocities are mapped into depth under some simplifying assumptions. White et al. (2003) proposed travel time inversion of reflected and refracted arrivals to create a velocity model, and then use them to perform composite prestack depth migration in two stages. Initially they migrate selected events from far offsets only, where separation between primaries and multiples or converted arrivals is clearer, and then use this simplified image to help interpret the result for migrating full-offset range, which is noisier but has higher resolution.

MY APPROACH TO SUB-BASALT IMAGING

Although the above-mentioned papers help in making the processing of data simpler, we find their approach questionable. Firstly, using a low-frequency source will severely hamper the resolution of the data and severely limit the scale at which we can image. Although large geological features can be imaged, the small-scale features that may be important for hydrocarbon exploration cannot be resolved due to the absence of the high-frequency content of the data. In addition, using refracted waves to build a velocity model has its limitations. To begin with, it is difficult to separate refraction and reflection data, and using refraction data from progressively deeper layers requires that with depth the velocity keeps increasing. This approach will fail in the case where there is a velocity inversion. If the velocity in a layer is lower than that of the layer above it

(Figure 1.2), no refraction will take place. Thus this velocity model will not be accurate, as the velocity of this layer will not be recorded. Another requirement for refraction data is that the interface between the layers is smooth. This is not true for most of the basalt basins where the basalt top and bottom are rough.

The method proposed by White et al. (2003) although helps in tying larger features observed in the far offset data with the near offset data, but due to the low resolution of far offset data, the smaller features that can be resolved in the high resolution of near-offset data will stay hidden. Also the noise in the near-offset data such as scattered multiples will still be present, making interpretation of the entire data difficult.

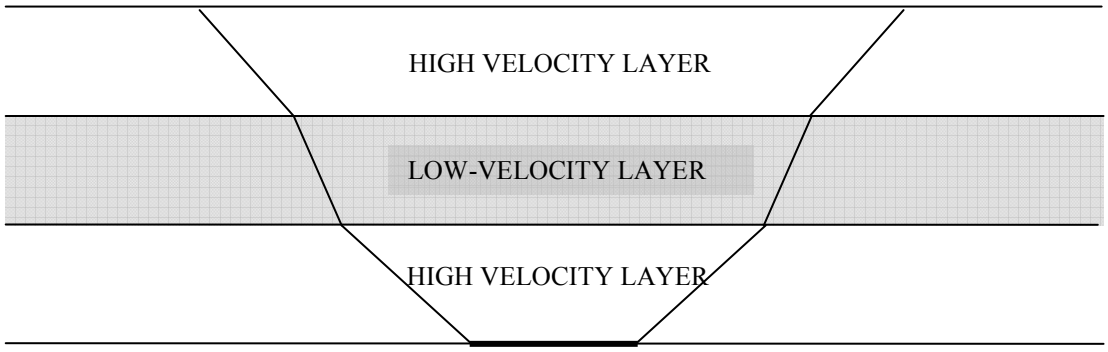

Figure 1.2: An illustration of seismic wave propagation while passing from a high velocity layer to the underlying relatively low-velocity layer. Note that no refraction takes place at this interface, as the critical angle required for refraction to take place cannot be achieved.

Another assumption that is questionable is that the far offset data are free of multiples, Fliedner and White (1999 and 2001). This is not true, as the recorded

refraction data may have bounced between two interfaces before or after being refracted, as shown in Figure 1.3a – 1.3c.

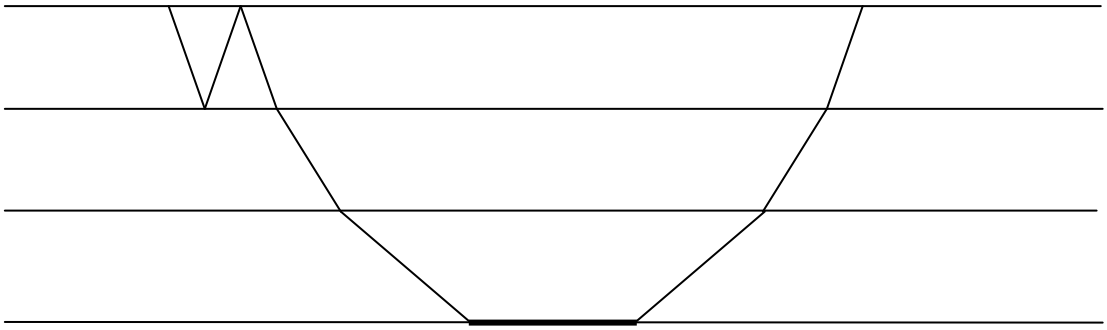

Figure 1.3a: An illustration of seismic waves undergoing multiple reflections between two interfaces before transmitting through the medium.

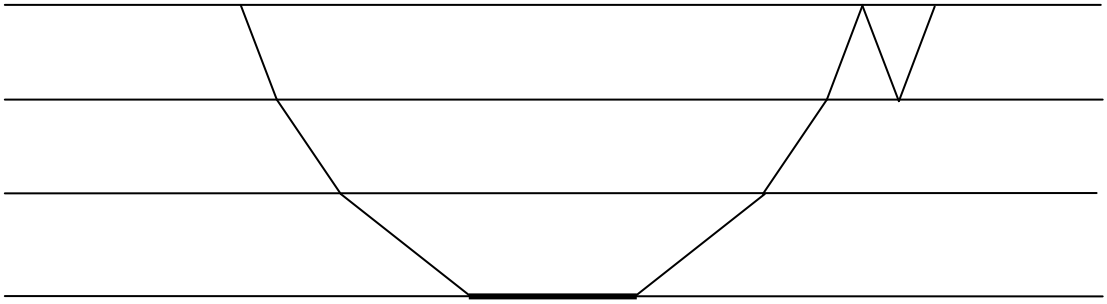

Figure 1.3b: An illustration of seismic waves undergoing multiple reflections between two interfaces after transmitting through the medium.

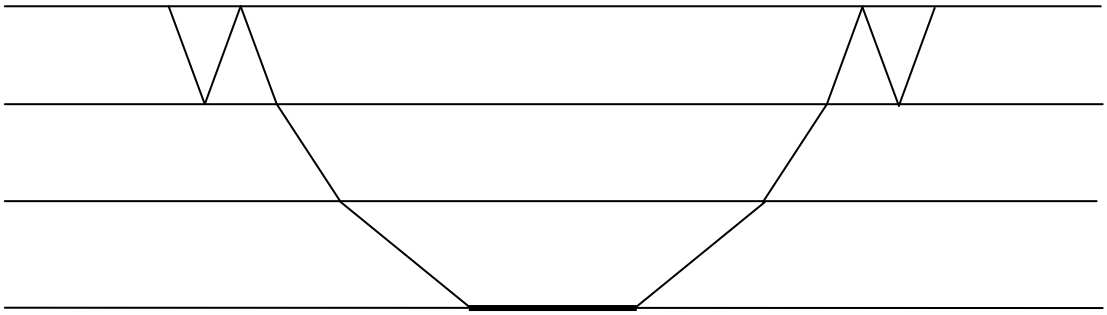

Figure 1.3c: An illustration of seismic waves undergoing multiple reflections between two interfaces before and after transmitting through the medium.

To improve the imaging of near-offset as well as far-offset data, we in this thesis, focus on studying the effect of processing techniques, in our case the multiple attenuation technique, in dealing with different heterogeneities in basalt. We classify the complexities in basalt into different categories and study the response of each of these categories to the multiple attenuation technique, which first predicts the multiples and then subtracts them from the data, using least-squares criteria. For example, the technique may effectively attenuate multiples for one category but fail to do the same for another category. Thus knowing the limitation of each process in dealing with the model will not only give us some insight into what that heterogeneity possibly is, but will also help us in coming up with optimum parameters to deal with the problem.

Choice of Acquisition Technique

In this thesis we have chosen OBS technique due to its advantages over the towed-streamer seismic (TSS) technique. Let us discuss the importance of OBS data that we are

going to use and the various events that are recorded in the OBS. OBS seismic requires that the sources be at the free surface (sea surface) while the receivers are at the sea floor (water bottom). This has various advantages over the towed-streamer seismic (TSS) where, in TSS the recorded waves are always P-waves (as the S-waves cannot transmit through water) while in OBS both P-waves and S-waves are recorded as the receivers are at the sea floor and the waves do not have to travel through water before reaching the receiver. Also we can record the vertical and horizontal components of particle velocity by using geophones in OBS data in addition to pressure data, which we get in TSS data. The problem of feathering that is encountered in TSS data acquisition is also avoided here. Another important advantage of using OBS data for the particular demultiple technique that we are going to employ is that the first multiple, which is the first order water-bottom multiple, is recorded much later than the primary of the same reflector as compared TSS data. This helps in defining a larger portion of data that contains primaries only. The advantage of this property again will be discussed in the next chapter.

The various events recorded in OBS data are primary reflections, direct waves, multiples, ghost and refractions (Figure 1.4) shows an illustration of typical raypath describing each of the events in OBS data). Compared to TSS data the events also have different implications on the method, e.g., the direct waves in OBS are indistinguishable from the primaries of the sea floor, as the receivers are positioned on the sea floor, receiver ghosts are indistinguishable from the primaries and multiples that have the last bounce at the sea floor.

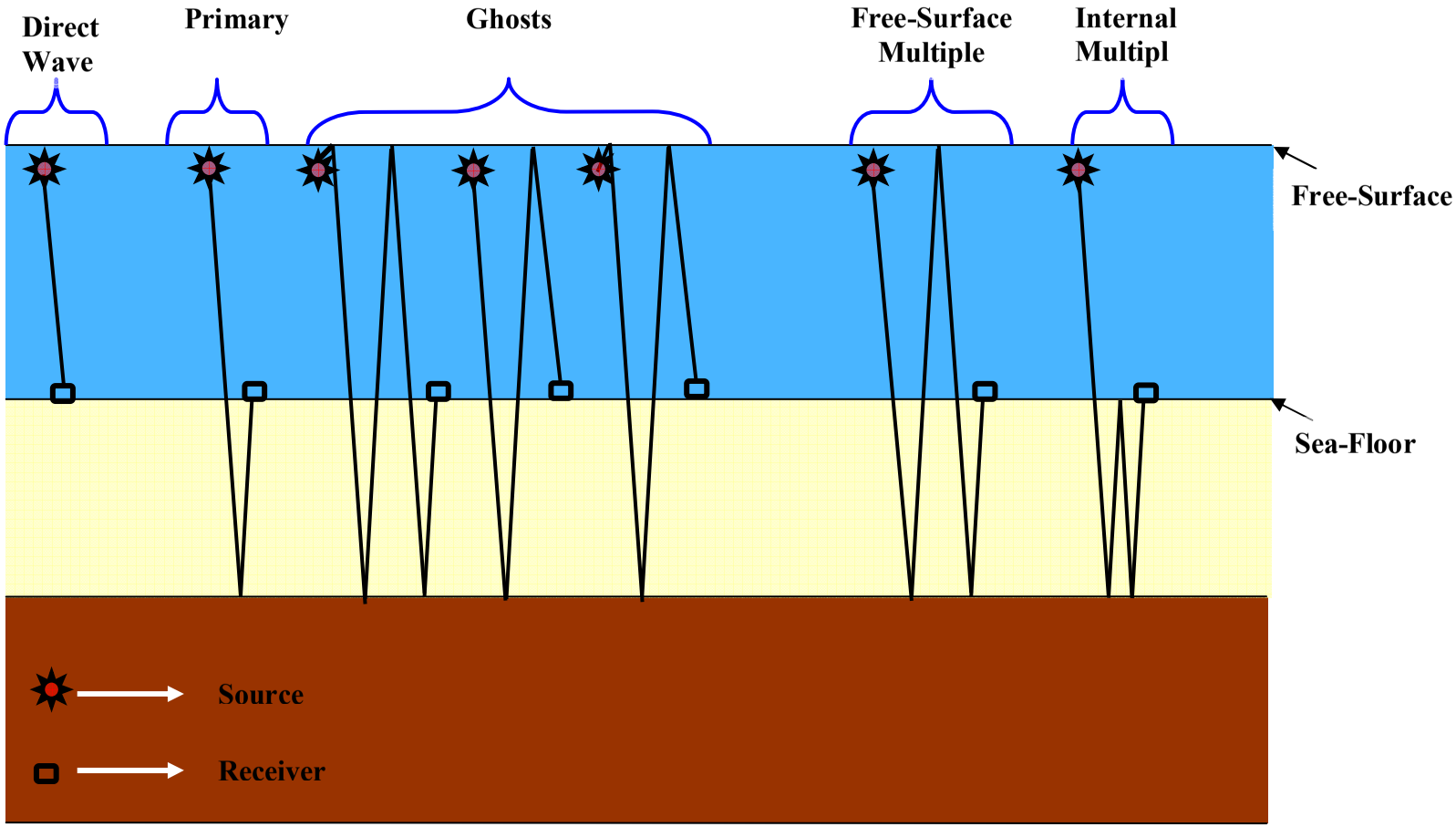

Figure 1.4: An illustration of various seismic events recorded in OBS seismic data.

ORGANIZATION OF THIS THESIS

In this thesis, we have built four models that incorporate all the features that are seen in a basalt basin (Figure 1.5) to study the problem of imaging sub-basalt horizons. Four models have been generated each having a different class of complexity. To compare the results, the only difference that has been made to the models is the nature of the complexity in the basalt layer. To simulate seismic wave propagation through these models, we have used the elastic finite-difference method for generating data. In this thesis we have focused on the application of a multiple attenuation technique, the Bottom Multiple Generator technique, which first predicts the multiples and then subtracts them from the data, using least-squares criteria, to test its applicability in each of the four cases. In the end we will be discussing the results obtained from them.

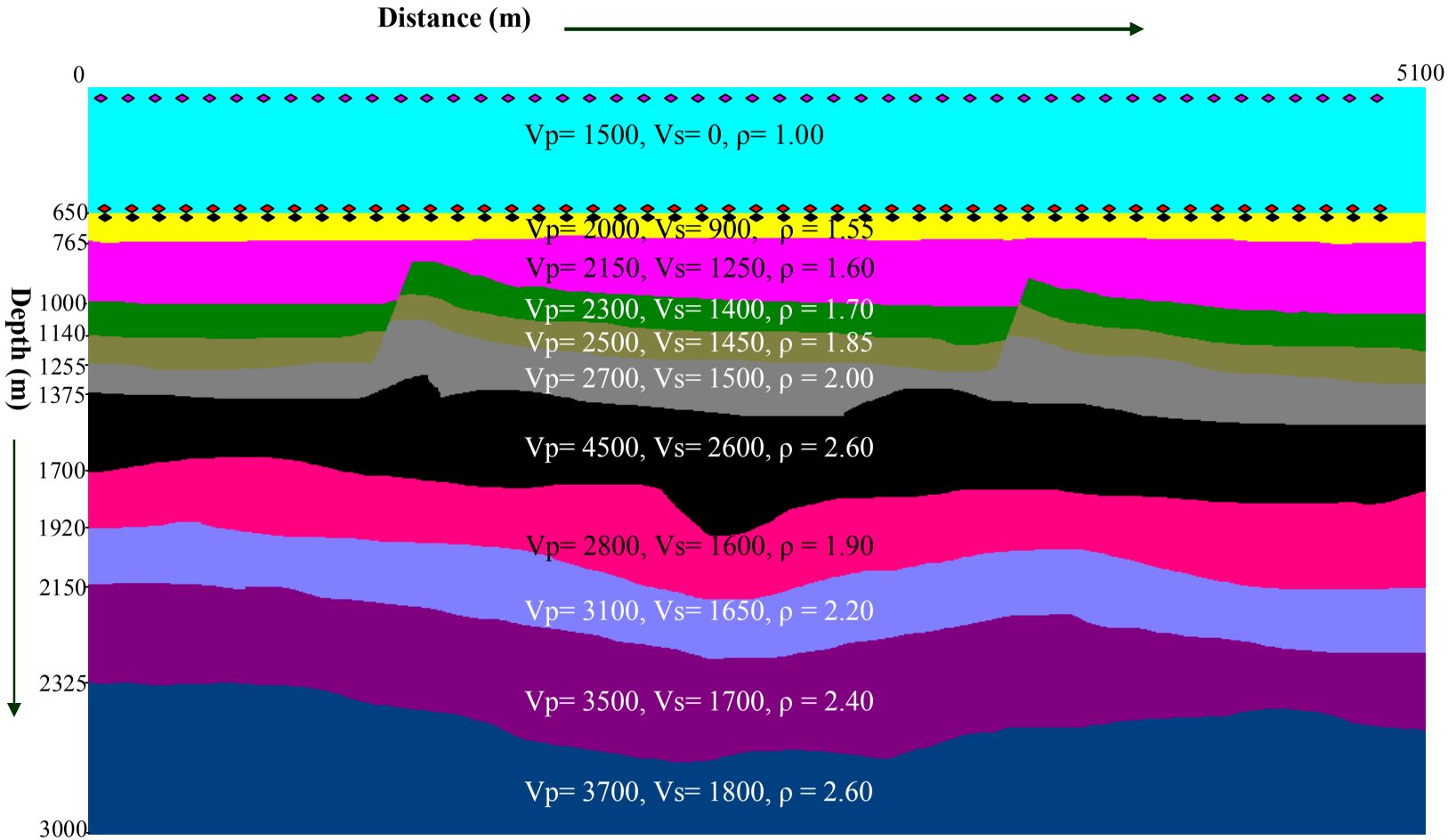

Figure 1.5: Model used to generate data using the elastic finite-difference method. Note that layer 7 is the basalt layer. Modern imaging technology is interested in imaging below this basalt layer. Velocities are in m/s, and density is in gm/cc.

CHAPTER II

UNDERSTANDING BASALT THROUGH THE FOUR MODELS

In the previous chapter we discussed the problems faced in the imaging of sub-basalt horizons due to the complex behavior of the basalt layer. If we can identify the cause of the problem that is hampering imaging of sub-basalt reflections, we can delineate the problems and focus on them. To delineate the problem, we have to understand the complexities in the basalt layer and classify them, based on the effect they have on the data. In this thesis we propose a way of categorizing the behavior of the basalt layer into four groups, based on its complexities. We study the response of each of these categories to the multiple attenuation technique, which first predicts the multiples and then subtracts them from the data using least-squares criteria. For example, the technique may effectively attenuate multiples for one category but fail to do the same for another. Thus, knowing the limitation of each process in dealing with the models will not only give us some insight into the complexities, but will also help us in finding optimal solutions to deal with the problems.

Sub-basalt imaging problems have several causes such as the following:

- High velocity and density of the basalt layers with respect to the surrounding sedimentary layers.
- Rough top and bottom of the basalt, causing significant multiple scattering.

- Poor signal to noise ratio of sub-basalt reflections due to multiple events generated from the top of the basalt and the inter-bedded units, representing different flows, within the basalt layer.
- Scattering energy and absorption from the small-scale heterogeneities in the basalt layer.

MODEL I

Let us discuss each of the above categories in more detail. Due to the high acoustic impedance contrast between the basalt and the surrounding sedimentary layers, primary waves (P-waves) traveling to the sub-basalt layers and then coming back up have to pass through the large sediment-basalt impedance contrast four times, twice while going down and twice while coming up (see Figure 2.1).

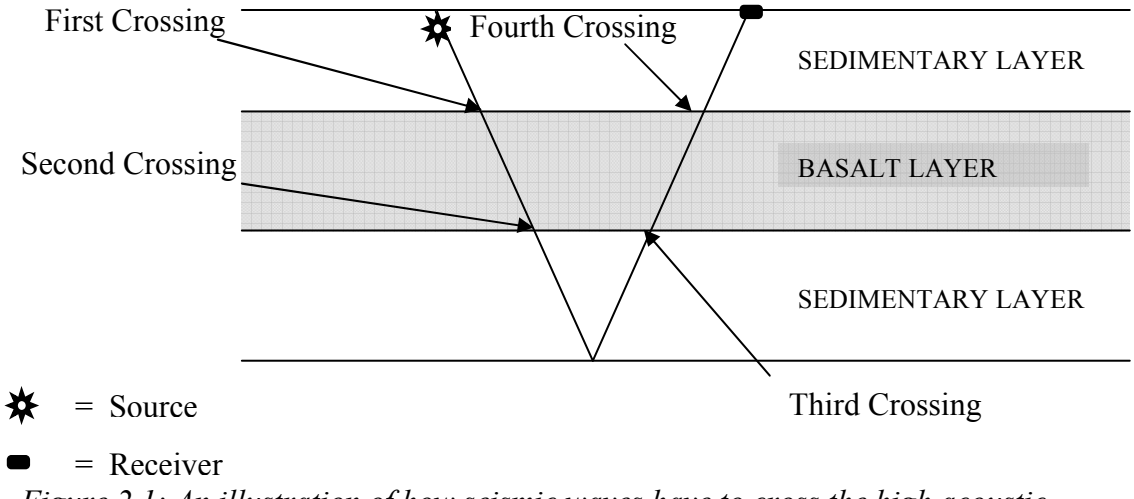

Figure 2.1: An illustration of how seismic waves have to cross the high acoustic impedance contrast boundary four times for the primary reflection from sub-basalt horizon to be recorded.

The high-impedance contrast leads to unusually weak sub-basalt primary reflections, as most of the energy is reflected back into the incident medium when the wave hits the sediment-basalt interface. In addition, the presence of a high-impedance contrast at the top of the basalt leads to strong free-surface multiples (FSM) between the basalt top and the free surface, and internal multiples (IM) between the basalt top and another strong reflector, e.g. sea floor (Figure 2.2). These FSM and IM interfere with the primary reflections from the sub-basalt horizons (Figure 2.3), making interpretation very difficult and sometimes even leading to misinterpretation of various events. Due to ringing, the multiples totally obscure the already-weak reflections from sub-basalt layers.

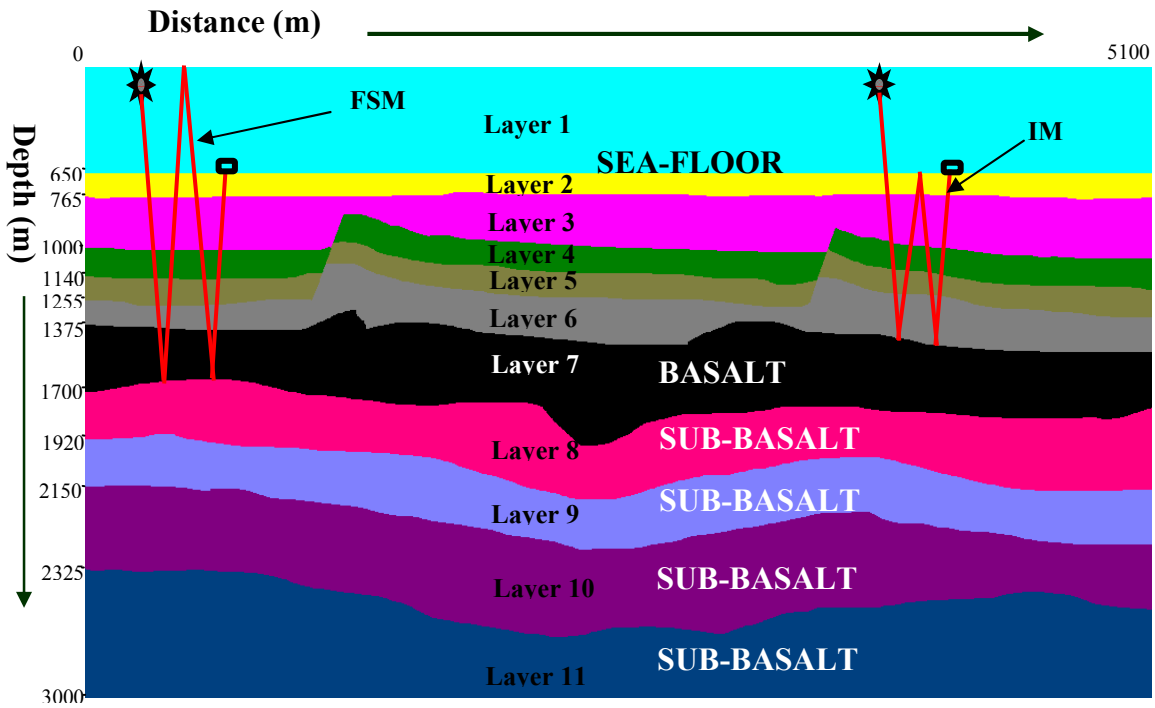

Figure 2.2: An illustration of the free-surface multiples between the basalt top and the free surface, and the internal multiple between the basalt top and the sea floor. FSM=Free-Surface Multiples and IM=Internal Multiples.

FSM from the top of the basalt is very strong and reflects most of the energy back to the surface. This makes the sub-basalt reflections (reflections from layers 9, 10 and 11) very weak and difficult to identify in a seismic section.

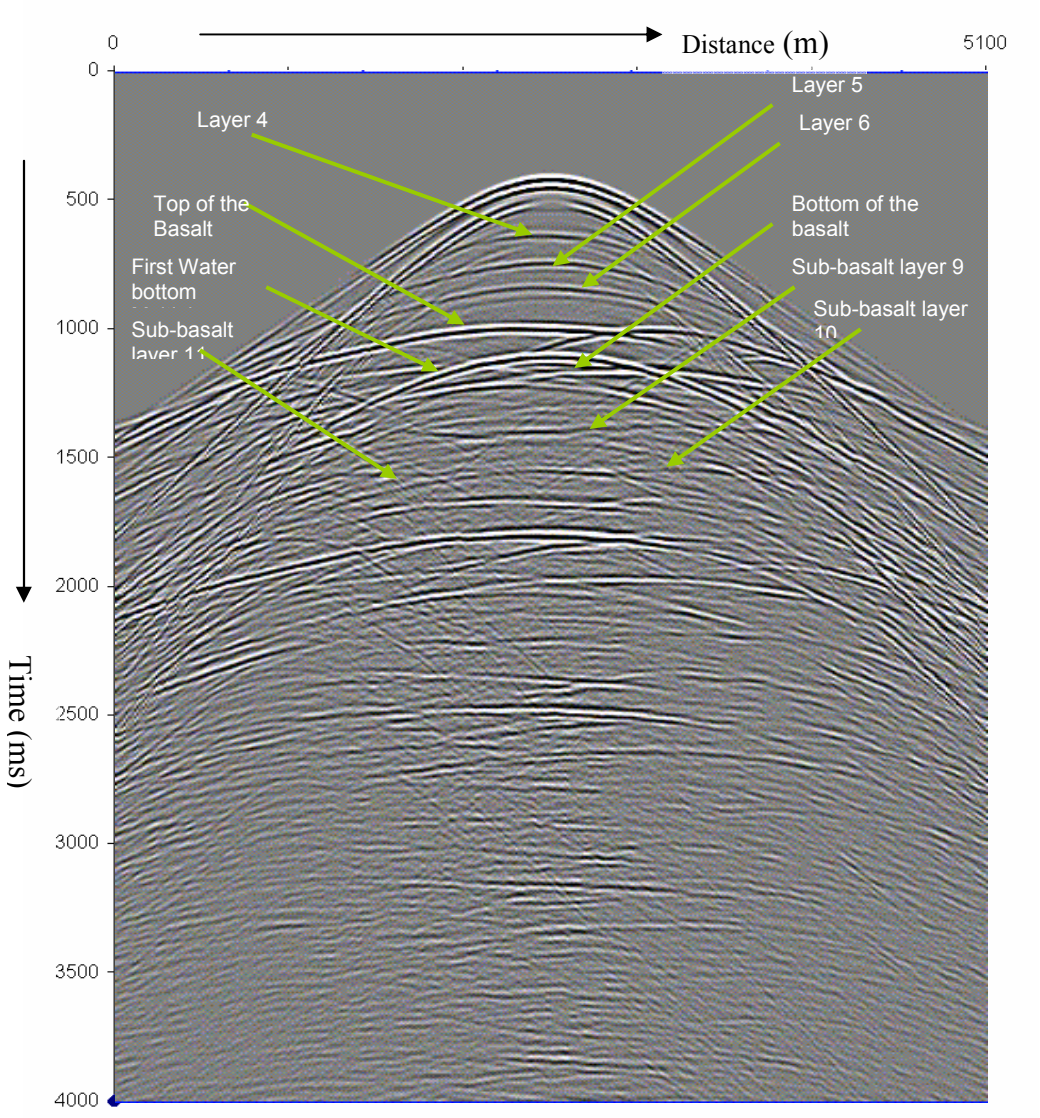

Figure 2.3: An illustration of a shot gather for the model discussed in Figure 2.2. Note that the reflections from layers above the first water bottom multiple can be easily seen while the reflections from the top of the sub-basalt layers 9, 10 and 11 that arrive after the arrival of the first water bottom multiple cannot be seen clearly as they are drowned in the noise of free-surface multiples of the overlying layers.

Thus, the above-mentioned complexity defines our first category, where the high acoustic-impedance contrast between the basalt and the surrounding sedimentary layers generates strong multiples. Note that high velocity and density are intrinsic properties of the basalt and will be present in all subsequent models.

MODEL II

To define the second category of basalt complexity, let us look at the top and bottom surfaces of the basalt layer. It is very common in the various basins mentioned in Chapter I for the basalt to have a very irregular surface. The roughness of basalt, like the basalt-top roughness and the valley fill at the bottom, etc., cause a significant energy scattering and absorption (Figure 2.4). These characteristics have a very detrimental effect on the data as multiple scattering from the top and bottom of the basalt layer degrade the signal-to-noise ratio even further.

A shot gather for Model II is shown in Figure 2.5. Note that the reflections from the top of the basalt are scattered due to its rough surface. The rough surface of the basalt also scattres the energy coming from the underlying reflectors thus making the events of the the sub-basalt reflectors very weak.

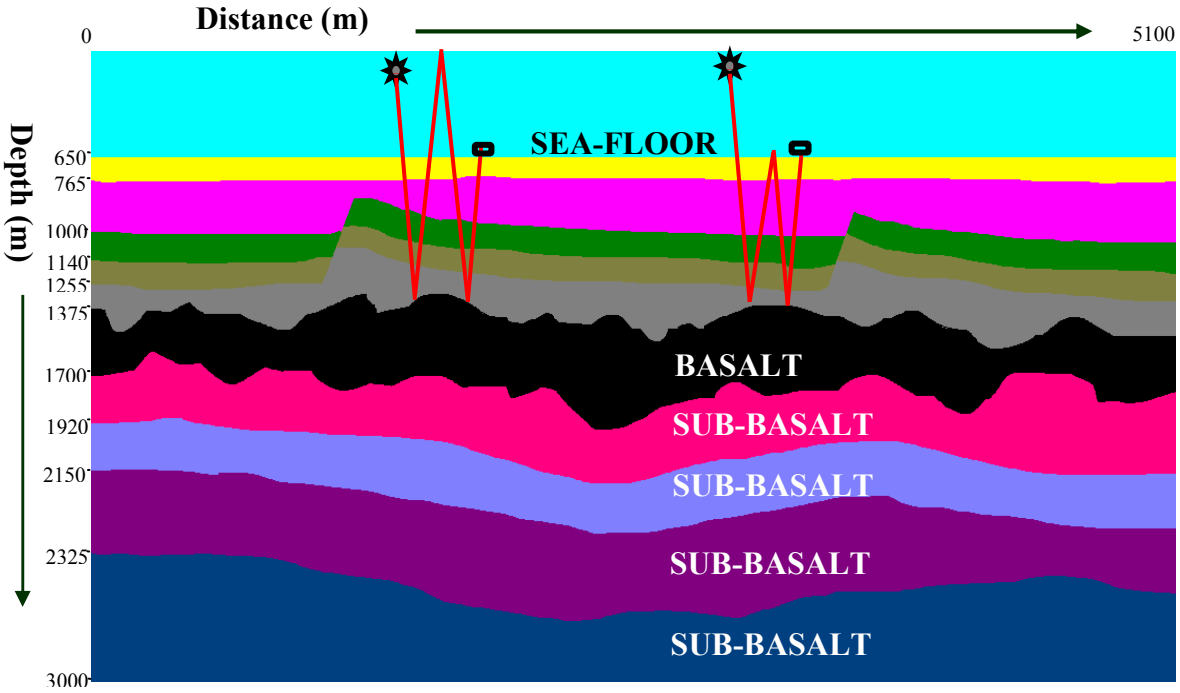

Figure 2.4: An illustration of the rough top and bottom of the basalt layer. Due to the roughness, the incident energy is scattered, degrading the signal-to-noise ratio of the data.

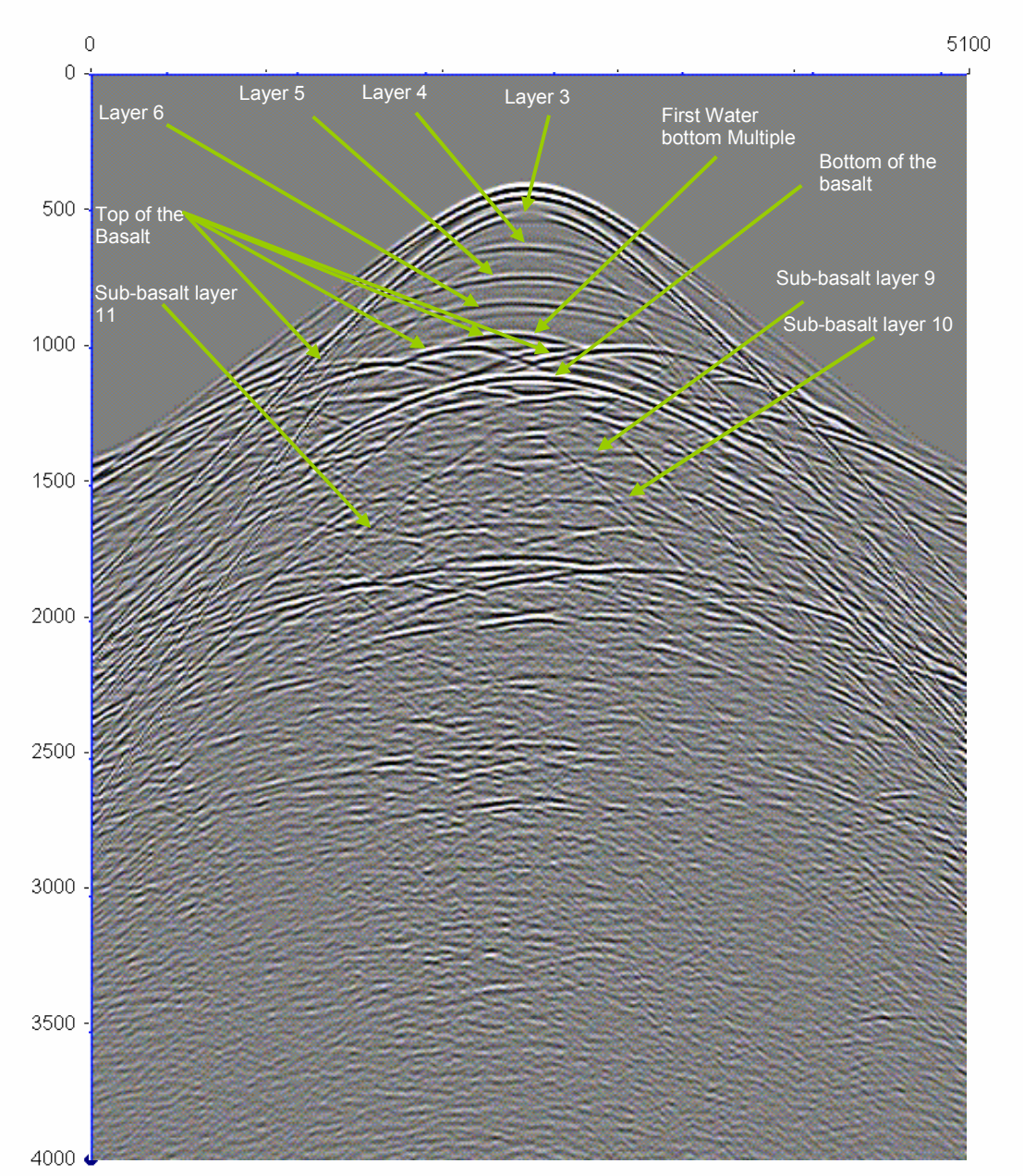

Figure 2.5: An illustration of a shot gather for the model discussed in Figure 2.4. Note that the reflection from the basalt layer is scattered due to the irregular surface of the basalt layer. Due to the rough surface of the basalt layer the events below it become very weak and difficult to image.

MODEL III

In the third model basalt deposits are found where magma has intruded the sedimentary rocks and has come to the surface. The intrusion of magma is not a continuous process but rather happens in spurts. With each event, a new layer of basalt, called a basalt flow, is deposited on top of the older one. Between each basalt flow, there is a time of non-deposition and erosion, which makes the top of each flow clayey in composition, thus reducing the density and velocity of this upper surface (Planke and Haugen, 2001). Due to this vertical variation in velocity and density within the basalt layer causes each flow to act like a reflector that scatters the energy (Figure 2.6).

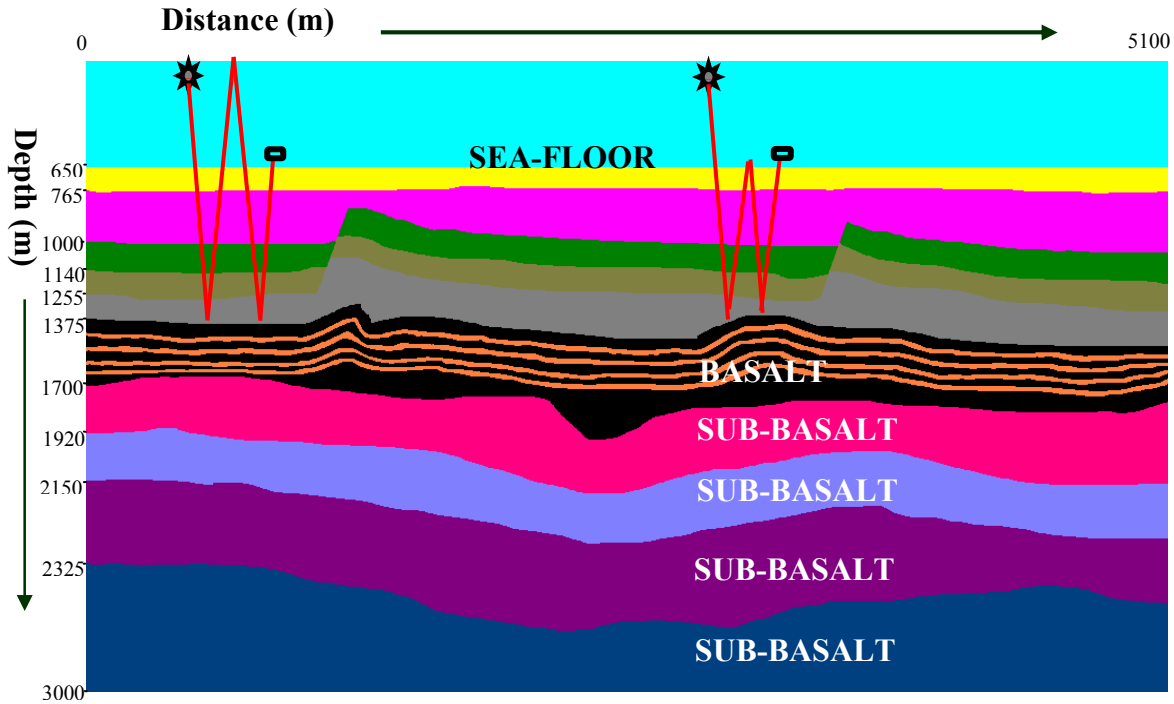

Figure 2.6: An illustration of vertical variation in elastic properties (velocity and density) within the basalt, caused by the weathering and erosion of the top of each flow.

The seismic data related to this model shows the effect of the basalt flows on it. The basalt flows act like closely spaced reflectors that are often below seismic resolution. These reflectors not only produce strong multiples as shown in Figure 2.7, they also obscure the sub-basalt reflectors making the seismic picture very noisy.

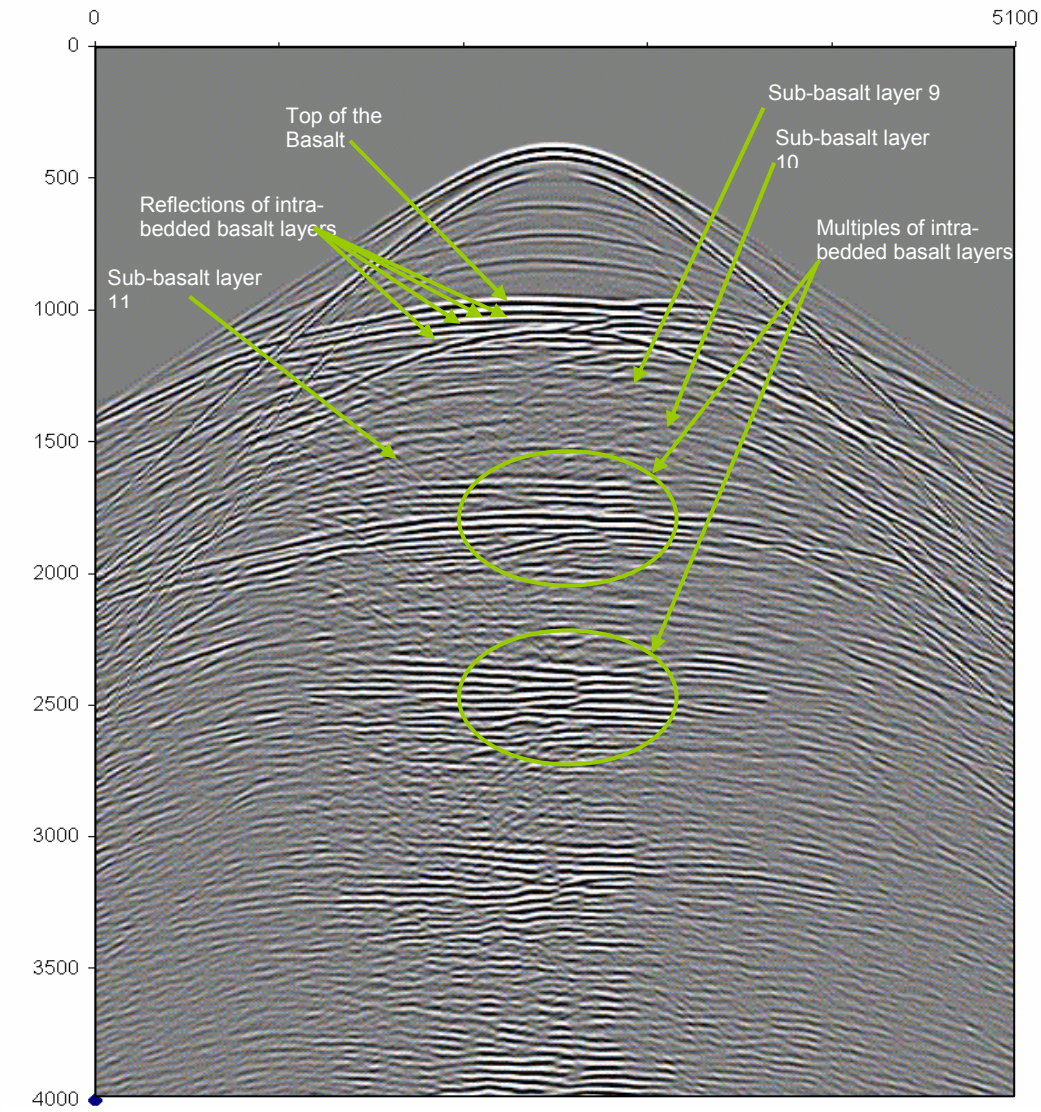

Figure 2.7: An illustration of a shot gather for the model discussed in Figure 2.6. Note that the strong multiples of the intra-bedded layers of basalt are totally obscure sub-basalt reflections. These intra-bedded layers also act as strong reflectors allowing very little energy to pass through them.

MODEL IV

Lastly, the fourth model contains several small-scale heterogeneities in the basalt, such as the presence of fractures and trapped bubbles (vesicular basalt), as shown in Figure 2.8. When the magma intrudes the sedimentary layers and comes to the surface, due to the low temperature at the surface, it undergoes rapid cooling. As a result the gases in the magma do not have enough time to escape and are trapped when the basalt is formed. The layer may also undergo fracturing after deposition due to external forces. These fractures and trapped bubbles act as small-scale heterogeneities that cause a significant absorption and scattering of seismic energy, making the data noisy.

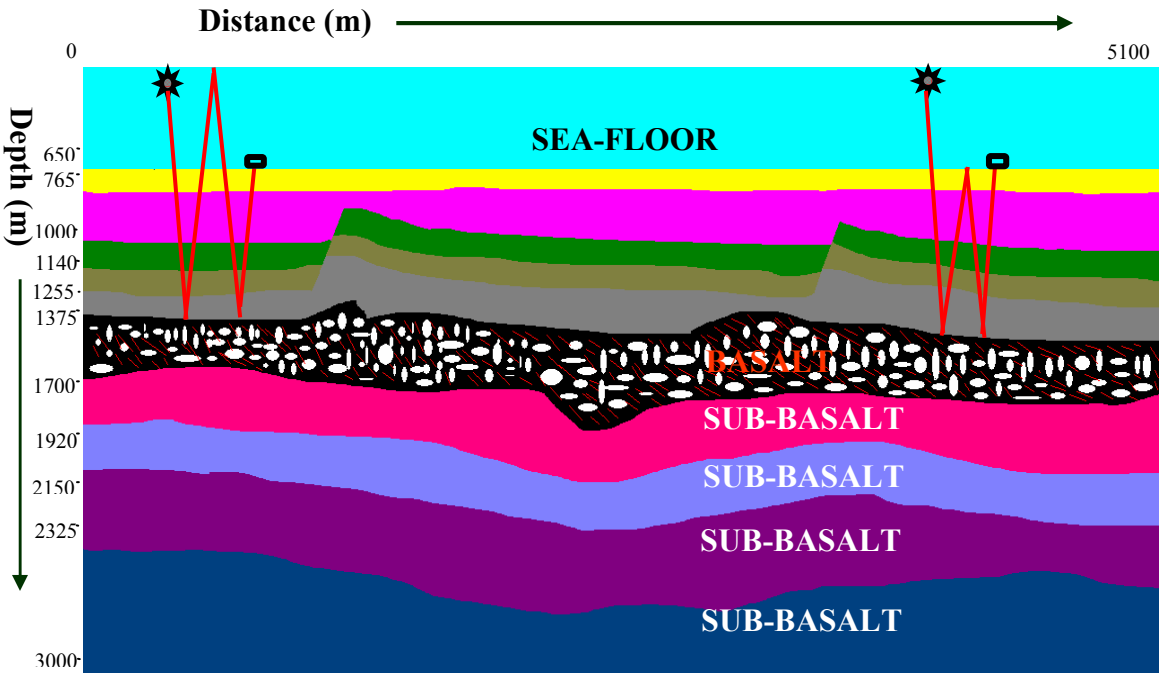

Figure 2.8: An illustration of small-scale heterogeneities like presence of gas bubbles and fractures in the basalt.

The seismic image of Model IV (Figure 2.9) gives a very fuzzy picture of the events below the basalt layer. This is due to scattering of energy when passing through the small-scale heterogeneities present within the basalt layer as shown in Figure 2.8. The sub-basalt reflections are totally immersed in the noise and are not visible in the seismic section.

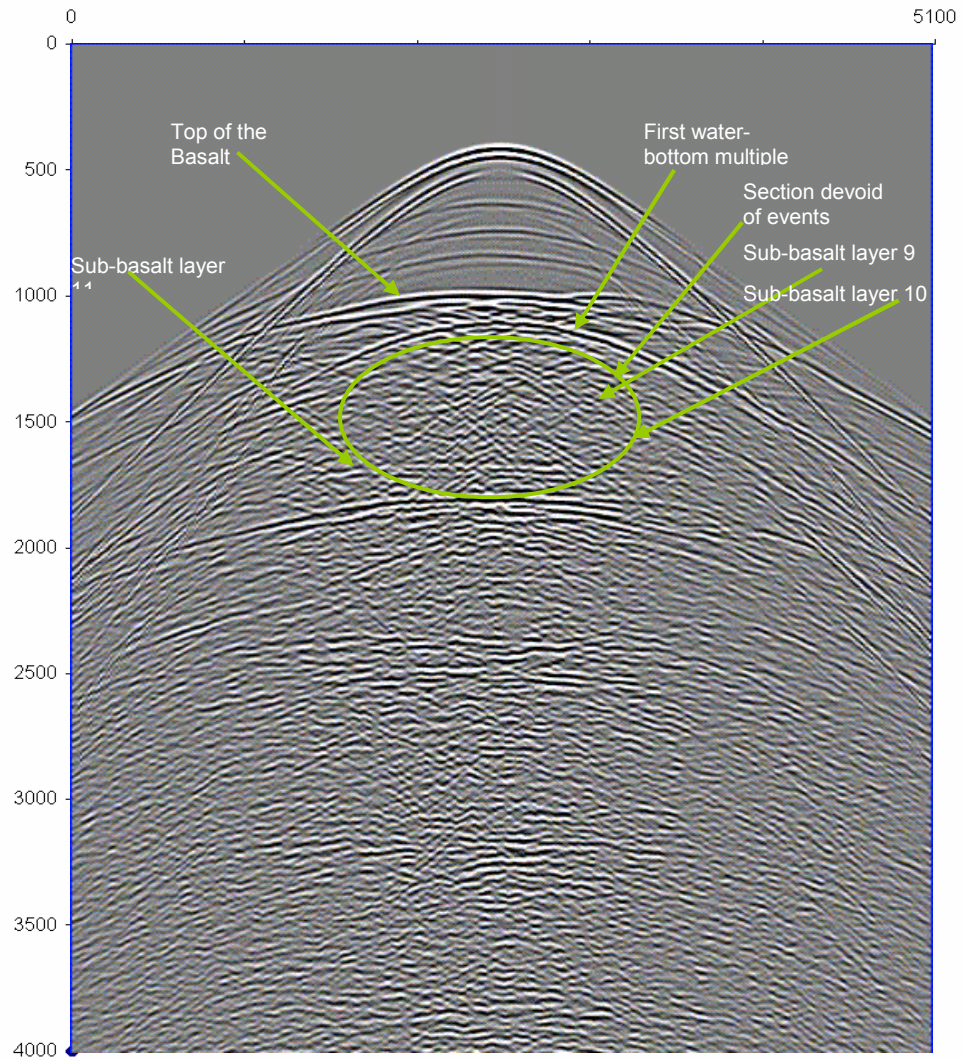

Figure 2.9: An illustration of a shot gather for the model discussed in Figure 2.8. Note that the small-scale heterogeneities in the basalt scatter the energy, making the underlying events very difficult to image.

We have classified the complexities of basalt into just four categories, each affecting the data in a different way. By so doing, we hope to illustrate that by knowing the limitation of each process, we can throw some light on optimal solutions for imaging the sub-basalt reflections. Note that the only change made to the models is to incorporate the nature of complexity. This will help us in determining the effect of each complexity on the data by comparing with each other.

Table 2.1 summarizes the characteristics of the four models discussed above. The classification can also be expressed graphically by using a part of the model that we will use for each of the cases, as shown in Figure 2.10.

Table 2.1: An illustration of the four models in tabular form based on the complexity present in each.

Basalt Complexity	Model I	Model II	Model III	Model IV
High-Impedance Contrast	High-Impedance Contrast	High-Impedance Contrast	High-Impedance Contrast	High-Impedance Contrast
Surface Roughness	Smooth	Rough	Smooth	Smooth
Small-Scale Heterogeneities	Absent	Absent	Present	Absent
Intra-Basalt Layering	Absent (No Velocity Variation)	Absent (No Velocity Variation)	Absent (No Velocity Variation)	Present

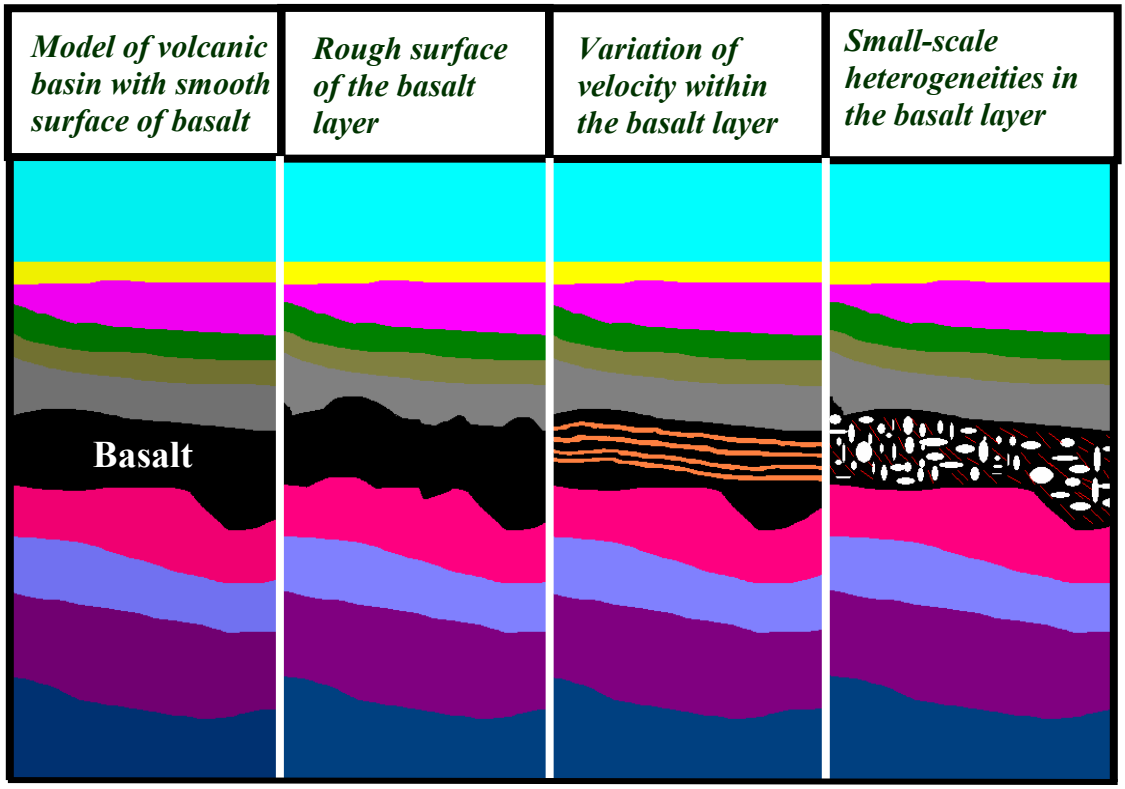

Figure 2.10: A graphical illustration of the four models based on the complexity present in each.

CHAPTER III

ANALYSIS OF SUB-BASALT IMAGING THROUGH DEMULTIPLE OF THE FOUR BASALT MODELS

We here present an analysis of sub-basalt imaging for the four basalt models introduced in Chapter II. Specifically we will analyze the effectiveness of the "predict and then subtract" technique for improving the imaging of sub-basalt reflectors.

As we discussed in Chapter I, it is useful, when aiming to analyze sub-basalt data, to record both P-wave and S-wave information. For this reason our analysis here will be carried out on OBS data. In fact, OBS data contain not only P-wave information, as in classical TSS data, but also S-wave information through sensors located at the sea floor.

The specific "predict and then subtract" demultiple technique we will use is known as bottom multiple generator approximation. Our formulation of this method is an adaptation to the OBS data that Watts (2005) described for TSS data.

FORMULATION OF THE DEMULTIPLE TECHNIQUE

The Predict and Then Subtract Technique

The formulation of the demultiple technique is based on the concept of "predict and then subtract" technology. The FSM are first predicted from the existing events and then subtracted from the data to attenuate the predicted multiples. To predict all the FSM only once, we need the solution given by the Kirchhoff scattering series.

If $\Phi = (p,v_x,v_y,v_z)$ denotes the four-component vector for OBS data, then the Kirchhoff scattering series (Ikelle and Amundsen 2003) is given by

$$\Phi_P = \Phi_0(x_r,\omega,x_s) + a(\omega)\Phi_1(x_r,\omega,x_s) + a^2(\omega)\,\Phi_2(x_r,\omega,x_s) + a^3(\omega)\Phi_3(x_r,\omega,x_s) + \ldots\ldots, \qquad (1)$$

where

$$\Phi_n(x_r, \omega, x_s) = \int_{-\infty}^{\infty} dx\, \Phi_{n-1}(x_r, \omega, x) \times E(x, \omega, x_s)$$

a = Inverse source signature

Φ_0 = OBS raw data

$a\Phi_1$ = aims at removing the first-order FSM. It predicts all the multiples that can be constructed using one scattering point.

$a\Phi_2$ = aims at removing the second-order FSM. It predicts all the multiples that can be constructed using two scattering points. Hence the first-order FSM cannot be predicted by $a\Phi_2$, as they have only one scattering point.

$a\Phi_3$ = aims at removing the third-order FSM. It predicts all the multiples that can be constructed using three scattering points.

E = TSS data with multiples

For more details on the construction of predicted multiples, refer to Appendix A.

Note that for construction of OBS predicted multiples, TSS data are also required. We generate TSS data along with OBS data. If we apply multidimensional convolution of TSS data with the OBS data, we will predict FSM of all orders (discussed in Appendix A), as the technique will compute all possible combinations. A FSM will be predicted more than once from different combinations of TSS and OBS data.

Linear Solution for Prediction of Multiples

The formula given in (1) can be used for multiple attenuation, though its solution is a series, which can be very time-consuming. For a more-efficient and stable solution, we need a linear equation for prediction of FSM. Ikelle and Amundsen (2002) found that the first term ($a\Phi_1$) of the series given in (1) predicted the first-order of FSM once. It predicted the second-order FSM twice, the third-order FSM thrice, and so on, as shown in Figure 3.1. The second term predicted the second-order FSM once, while it predicted the third-order FSM twice, the fourth-order FSM thrice, and so on, as shown in Figure 3.1. Note that the second term and the higher terms do not predict the first-order FSM. This property will be used in the estimation of the source signature as discussed in Appendix B. Thus if we add all the terms as given in (1), we can predict all the free-

surface multiples. The prediction algorithm computes all possible combinations of events in the data that follow Snell's law* and can be joined at the free surface to predict the multiples. Higher order (fourth-order onwards) FSM will be too weak to really affect the data and can be ignored. This series can attenuate the FSM effectively but is very time-consuming and unstable, as it is nonlinear.

However, if the TSS data are free of FSM, then the second term ($a\Phi_1'$) of the Kirchhoff series will still predict all orders of FSM, but they will be predicted only once. Thus we now have a linear solution to the problem in which subtraction of the predicted multiples from the data will give us the required result of data free of FSM.

$$\Phi_P(x_r,\omega,x_s) = \Phi_0(x_r,\omega,x_s) + a(\omega)\,\Phi_1'(x_r,\omega,x_s), \qquad (2)$$

where,

$$\Phi'_1(x_r, \omega, x_s) = \int_{-\infty}^{\infty} dx\, \Phi_0(x_r, \omega, x) \times E'(x, \omega, x_s)$$

E' = TSS data without FSM

---

* - *Although the figures shown in this thesis do not follow Snell's law, the algorithm takes Snell's law into account*

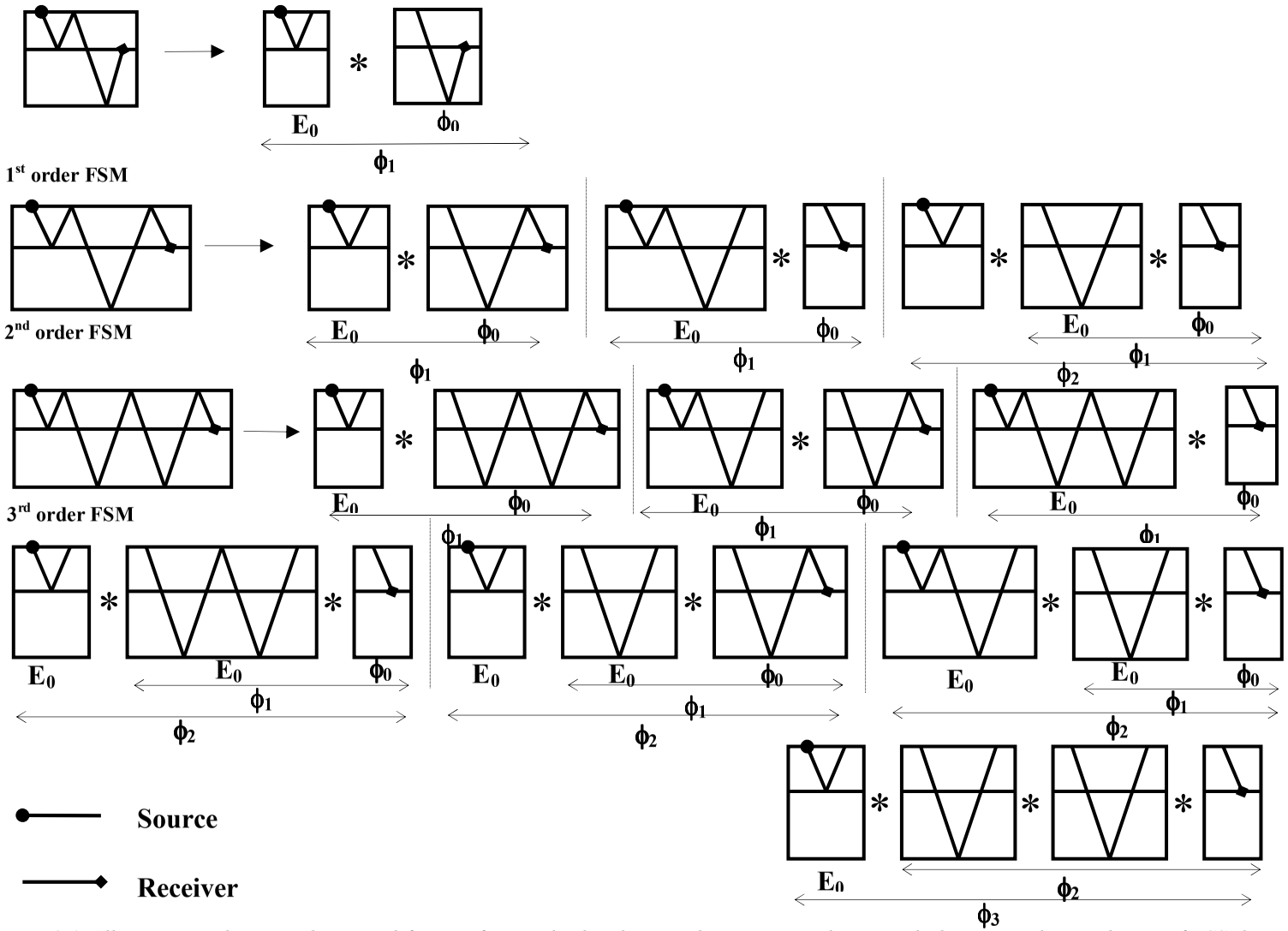

Figure 3.1: Illustrations showing ghosts and free surface multiples that can be represented as a multidimensional convolution of TSS data and OBS data. Notice that the first-order FSM is predicted only once by ϕ_1. The second-*order FSM is predicted two times by ϕ_1 and once by ϕ_2. The third-order FSM is predicted three times by ϕ_1, three times by ϕ_2, and only once by ϕ_3. Here E_0=TSS primary and ϕ_0=OBS raw data.*

Bottom Multiple Generator Approximation

The problem is to find a way to generate TSS data that contain primaries and no FSM. We have adapted the BMG solution proposed by Ikelle et al. (2004) for TSS data to OBS data for FSM attenuation. Although the solution given by Ikelle is a two-step approach we have used just the first step, as we think that the first step should be able to get rid of all the FSM in the case of deep water. This approach divides the TSS data into two parts by a hypothetical reflector (the BMG reflector) such that the primary associated with the BMG reflector arrives at the same time as the first-order water-bottom multiple (the first multiple recorded in the data). Thus the BMG reflector defines a part of the data above it that contains primaries only. The first step is to compute the multidimensional convolution "$\widetilde{\Phi}_1$" of the raw OBS data with the portion of TSS data containing primaries only (E_{BMG}), as given by (3). Then $\widetilde{\Phi}_1$ will predict all orders of FSM whose first bounce is above the BMG reflector, and they will all be predicted only once (Figure 3.2). Scaling the field of predicted FSM by the inverse of the source signature and subtracting it from the raw OBS data will attenuate all the FSM whose first bounce is above the BMG reflector (Figure 3.3).

$$\widetilde{\Phi}_1(x_r, \omega, x_s) = \int_{-\infty}^{\infty} dx\, \Phi_0(x_r, \omega, x) \times E_{BMG}(x, \omega, x_s) \tag{3}$$

where,

E_{BMG} = Portion of TSS data above the BMG containing no FSM

The final demultiple data will then be given by (4)

$$\Phi_P(x_r,\omega,x_s) \approx \Phi_0(x_r,\omega,x_s) + a(\omega)\ \widetilde{\Phi}_1(x_r,\omega,x_s), \qquad (4)$$

If the depth of the water column is large, as is the case in the basaltic basins which are found in deep water, the arrival for the first water-bottom multiple will be late, allowing most of the primaries to be incorporated in the portion of data above the BMG reflector. This will help us in predicting all the multiples related to these primaries.

In the case where not many primaries lie above the BMG reflector, to incorporate more primaries in the TSS data we apply the above step to the TSS data itself. By attenuating the multiples in TSS data, we can define a larger portion of data containing primaries only, which can be used for multidimensional convolution with the OBS data.

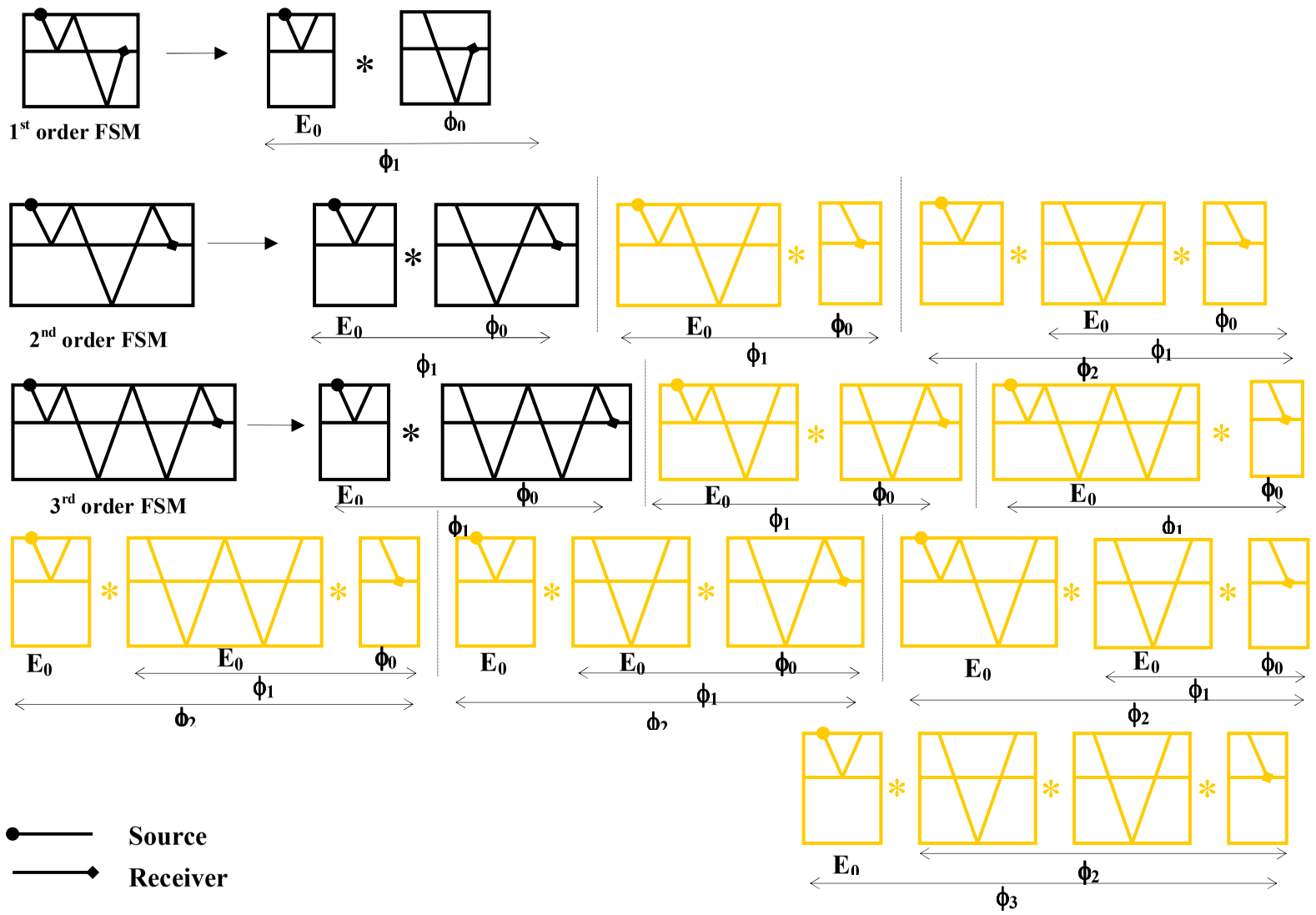

Figure 3.2: Illustrations of how ghosts and free surface multiples can be represented as a multidimensional convolution of TSS data and OBS data. Notice that by applying the BMG technique we only predict the FSM once.

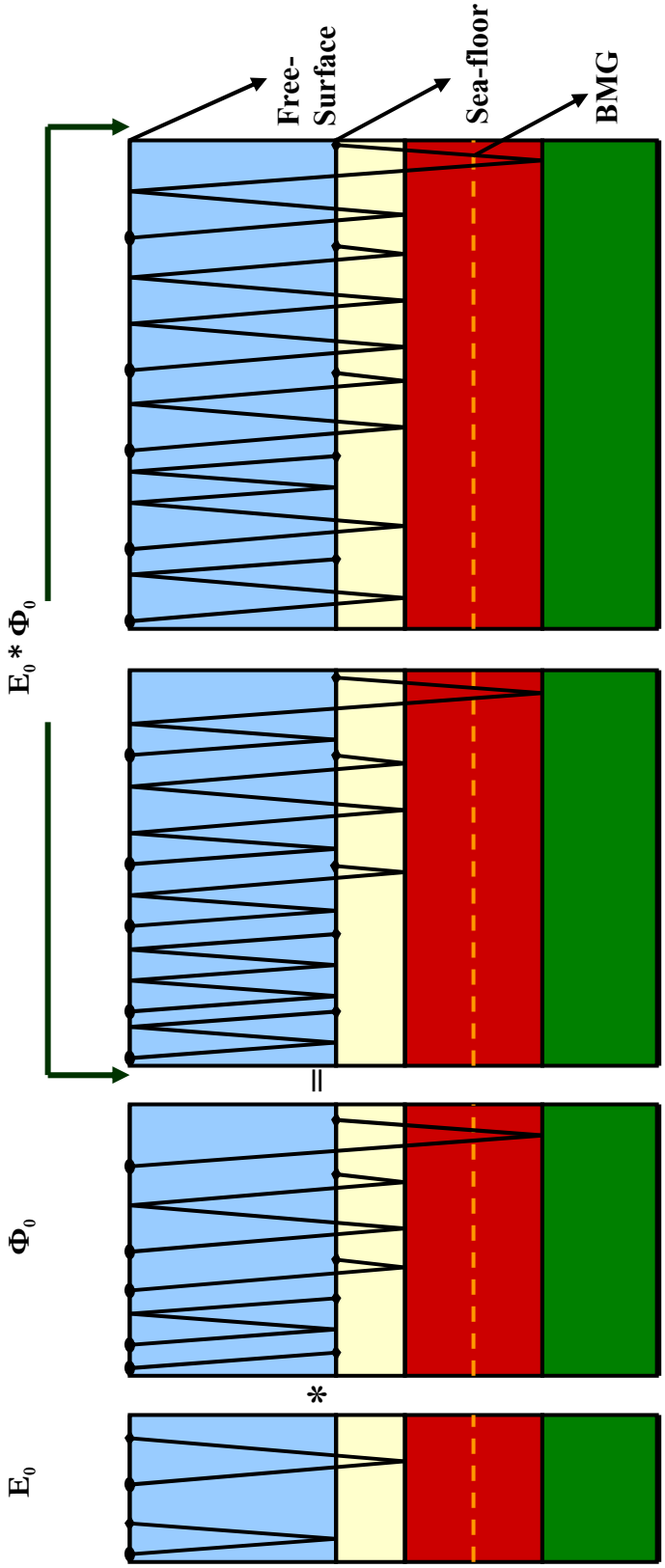

Figure 3.3 An illustration of FSM prediction for OBS data. These predicted FSM can be subtracted from the raw OBS data to attenuate FSM whose first bounce is above the BMG.

ANALYSIS OF RESULTS

Description of Data

Generation of OBS data for the four models described in Figures 2.2, 2.4, 2.6, and 2.8 was done using elastic finite difference modeling (Bayliss et al. 1986 and Graves, 1996). Specific elastic parameters used for this model are shown in Figure 3.4. Note that for the models in Figures 2.6 and 2.8, the elastic parameters used for intra-basalt heterogeneities are different from the rest of the models. Table 3.1 gives a detailed description of the parameters used for the basalt layer.

Table 3.1: An illustration of parameters for the four basalt models in tabular form based on the complexity present.

Basalt complexity (vel in m/s and density in g/cc)	Model I	Model II	Model III	Model IV
Basalt parameters	Vp = 4500 Vs = 2600 ρ = 2.6	Vp = 4500 Vs = 2600 ρ = 2.6	N/A	Vp = 4500 Vs = 2600 ρ = 2.6
Vesicular basalt	N/A	N/A	N/A	Vp = 4250 Vs = 2000 ρ = 1.9
Fractures	N/A	N/A	N/A	Vp = 2200 Vs = 1100 ρ =1.7
Intra-bedded units in basalt	N/A	N/A	Vp = 2800 Vs = 1600 ρ = 1.9	N/A

OBS data were generated with three components (P, V_x, V_z) for a fixed receiver array of 5100m. The distance between the receivers is 15 m. Three hundred and forty one (341) shots were generated with the same spacing as the receivers i.e. 15 m. We set up the configuration such that the X-position of the sources is identical to the X-position of the receivers

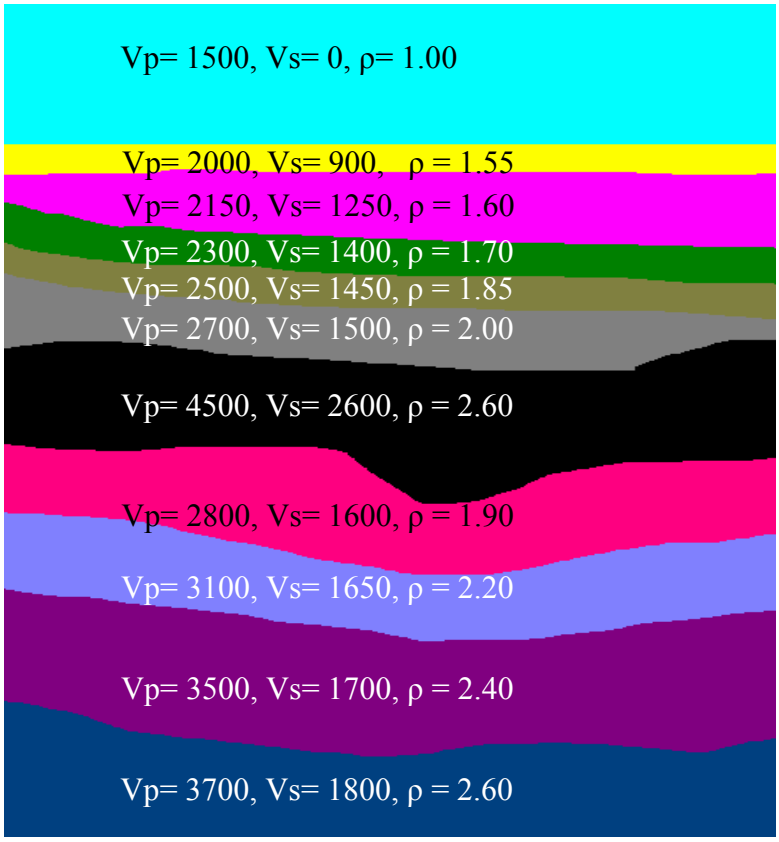

Figure 3.4 A graphical illustration of elastic parameters used in the four models. Note that for Model III and Model IV the elastic parameters are different for basalt layer. Vp indicates P-wave velocity in m/s, Vs indicates S-wave velocity in m/s, and ρ indicates density in g/cc.

As we have seen in the previous section, formulation of the OBS demultiple technique requires TSS data, so we recorded them along with our OBS data with the same source position. The TSS receiver array was placed near the free surface exactly above the OBS sensors.

In the first example we will describe the numerical implementation of the formulae discussed above. We will be applying the same formulae to the other three models. Note that we have applied exactly the same parameters for all the models for the comparison of the results.

The TSS data contain direct waves that are not required for the processing of data to avoid predicting ghosts. Hence the first step is to remove the direct waves. Figures 3.5a and 3.5b show data before and after the removal of direct waves.

The second step is to define the portion of the TSS data above the BMG reflector (E_{BMG}). We investigated two approaches for the defining the portion of data containing primaries only. The first is similar to the approach proposed by Ikelle and Amundsen (2004) for the demultiple of the TSS data that required prediction of the TSS multiple and then the use of these predicted multiples to define the BMG for muting of TSS data as illustrated in Figure 3.6a. Figure 3.6b shows the result of muting the data. The advantage of this method is that it very accurately and completely defines the portion of data containing primaries only. But this method has a drawback also, where it requires predicting the multiples for TSS data in order to cut it, the prediction process is very time-consuming and can be costly. The approach that we adopted in this thesis is to simply cut the data up to certain time where we feel confident that the data contain only

primaries. Therefore we avoid processing the data for predicting the multiples for TSS data, just to define the BMG. This process of simply cutting data is not as prone to errors as the first FSM, the water-bottom multiple, is easily identifiable. A comparison of the two approaches is shown in Figure 3.7. From the results, it is apparent that our approach worked well for predicting multiples for deep-water data.

After defining the TSS data containing primaries only, the next step is to predict the multiples for OBS data using (3). E_{BMG} is convolved with the OBS raw data shown in Figure 3.7b to predict the OBS FSM. Figure 3.8a shows the field of predicted multiples. Finally, we subtract the predicted multiples from the raw OBS data using (4), as shown in Figure 3.8b. The technique implemented for estimating the scaling factor $a(\omega)$ is described in Appendix B.

Before we start analyzing our results, let me reiterate that the process applied to Model I has been applied to all the other models, and exactly the same parameters were applied to all the models. Therefore, from now onward, we will analyze the demultiple results of the four models without describing the numerical steps for each case.

Let us start with the analysis of how effectively the sub-basalt layers are defined for the Model I after the demultiple.

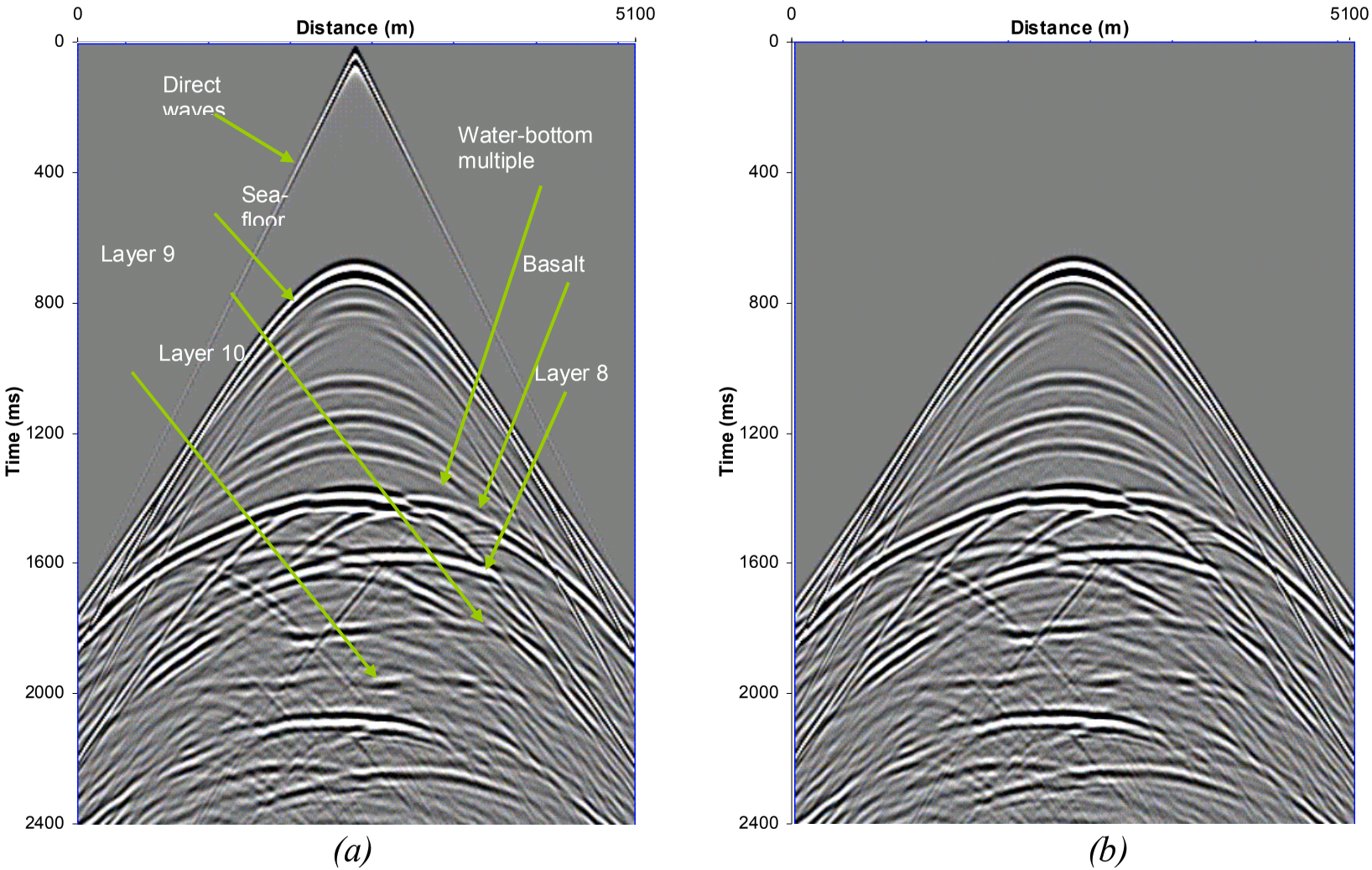

Figure 3.5: An illustration of TSS shot gather through Model I discussed in Figure 2.2. Direct waves can easily be identified here in (a).(b) shows TSS data without the direct waves. Note that data have been zoomed in to show the first 2400 ms.

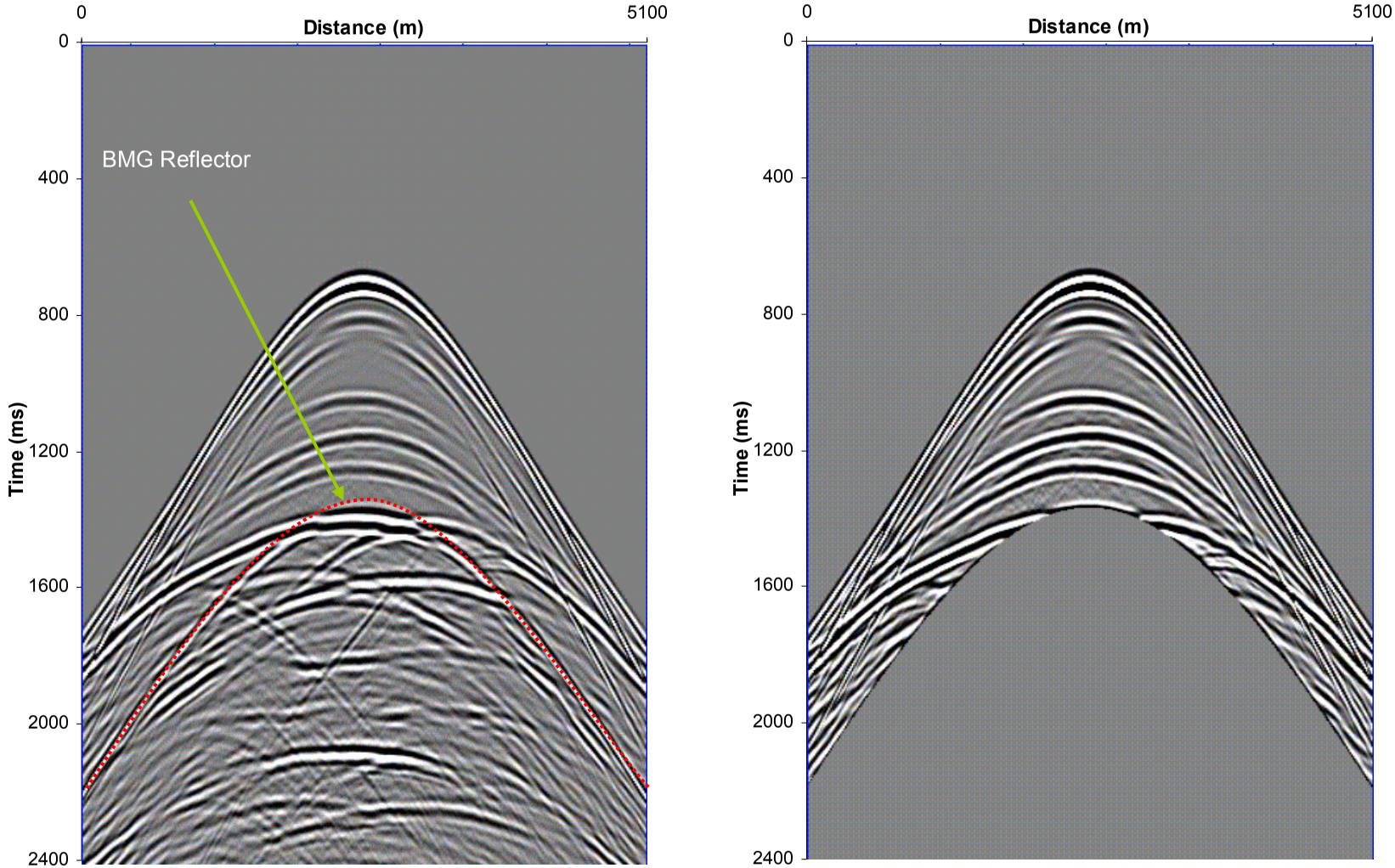

Figure 3.6: (a) Illustration of the definition of the BMG reflector. It coincides with the first FSM in the data, i.e. the water-bottom multiple. (b) Illustration of the *data after muting that data at the BMG.*

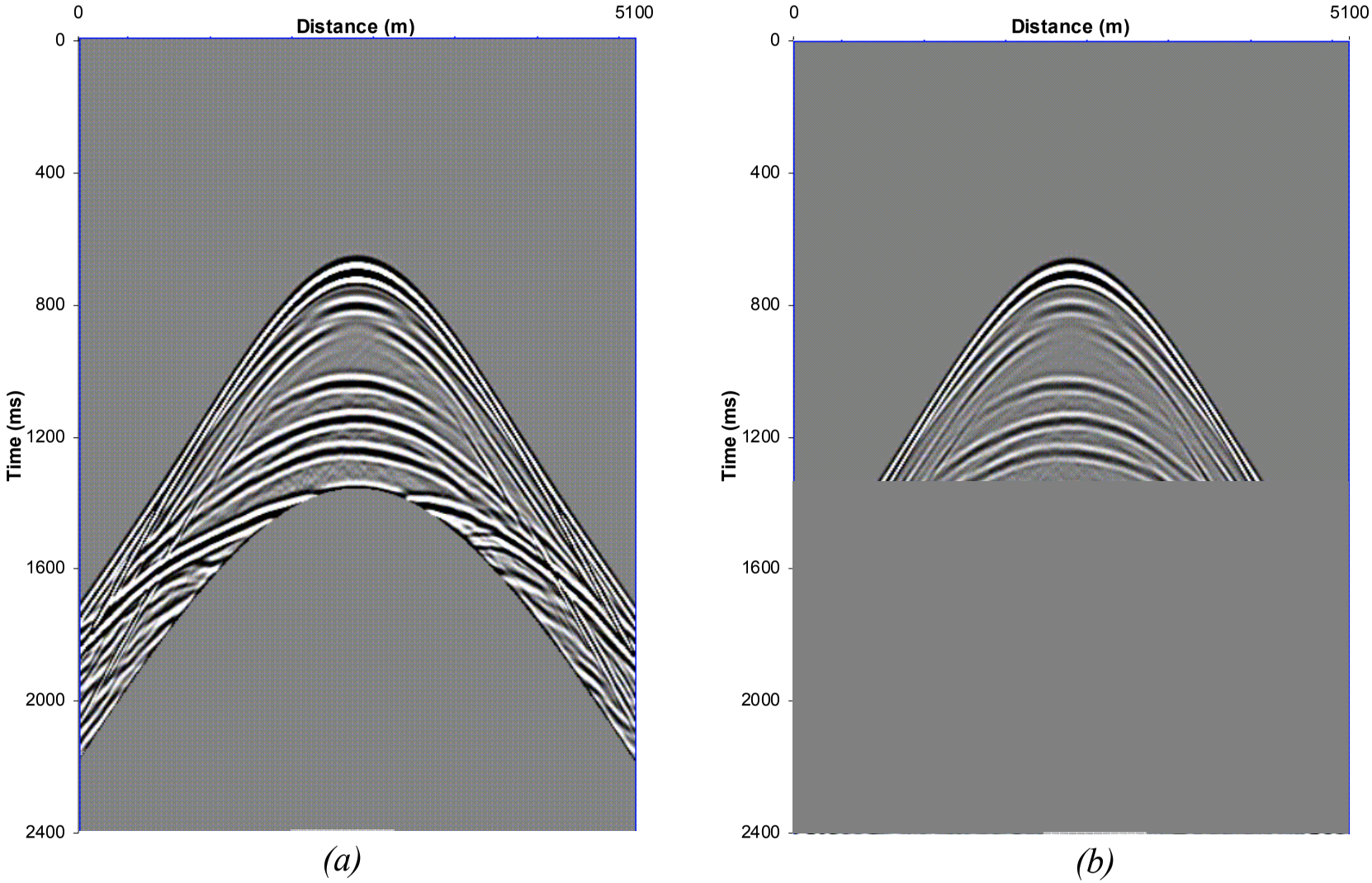

Figure 3.7: The above figures demonstrate the two ways of applying the BMG technique. (a) shows the classical way of defining the BMG accurately. (b) shows a more practical approach for defining data containing primaries.

MODEL I

Roughly speaking, the sub-basalt layers are visible in the raw OBS data in Figure 3.6 but are severely distorted by the interference between the primaries and the multiples. As we can see in Figure 3.9b of the predicted multiples, there are multiples with significant energy passing across the area where the sub-basalt layers are more clearly defined after the demultiple (Figure 3.10b). Moreover we can notice how continuously some of the sub-basalt layers are defined across the section.

To clearly illuminate this point, we have prepared zero-offset sections of the data. Figure 3.11 shows that all the multiples recorded in the raw data (a) are the also predicted in (b). Figure 3.12 is a zero-offset section of Figure 3.9, showing clearly, the improvement in the quality of the data after demultiple. We have zoomed the window of the data containing layers 9 and 10 (Figure 3.13). Notice how continuous sub-basalt layer 10 is across the entire section of the demultiple data. Such continuity is not visible in the raw data.

Therefore we conclude that sub-basalt imaging corresponding to Model I is possible with the current technology such as the one described in this chapter. In other words the current demultiple technique is suitable for sub-basalt imaging in places where basalt is almost homogeneous and has a smooth top and bottom, such as in the Angola basins.

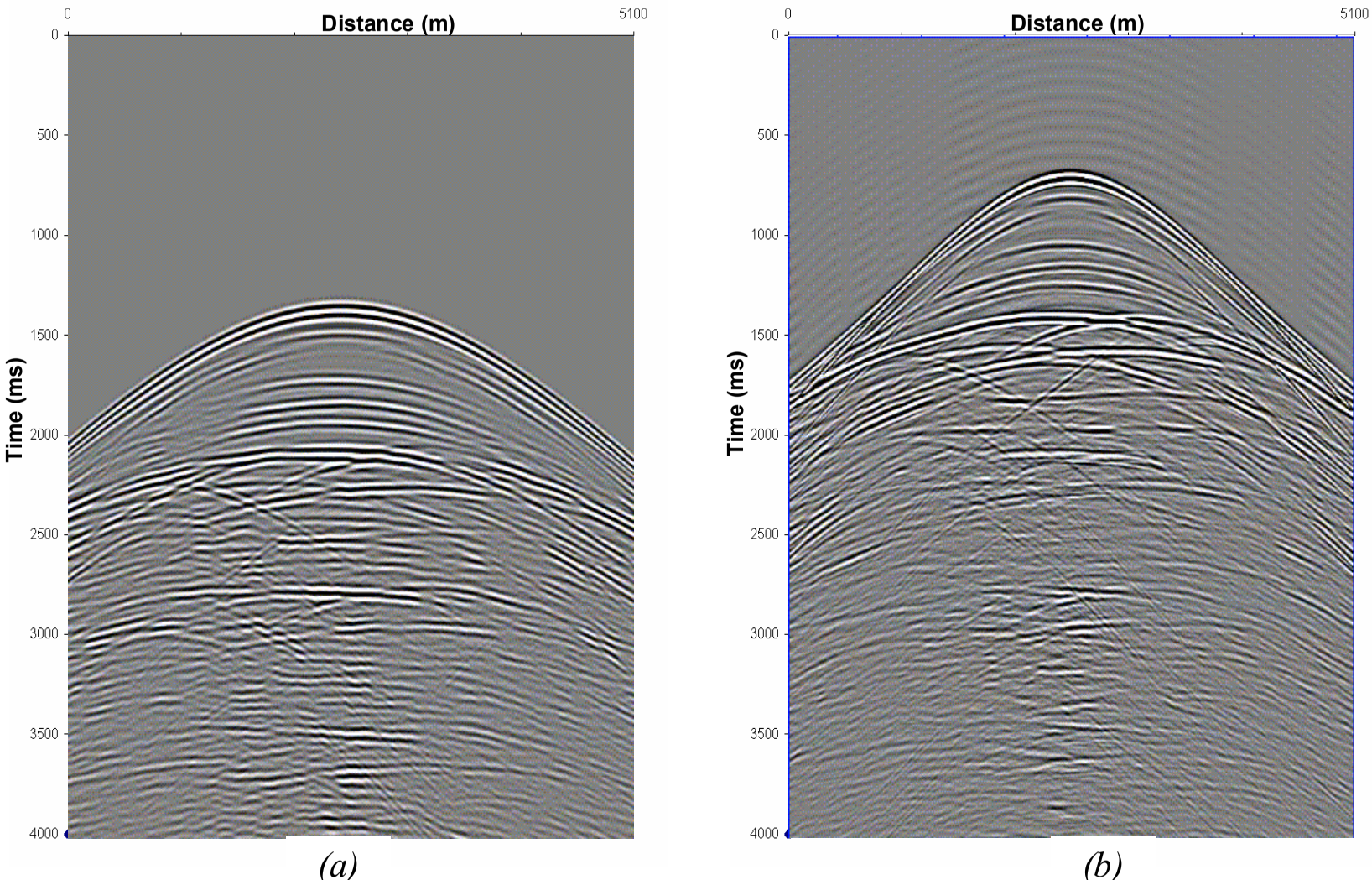

Figure 3.8: (a) Illustration of the predicted multiples for TSS data. (b) Illustration of the demultiple TSS data after the subtraction of the predicted TSS multiples in (a) from raw TSS data.

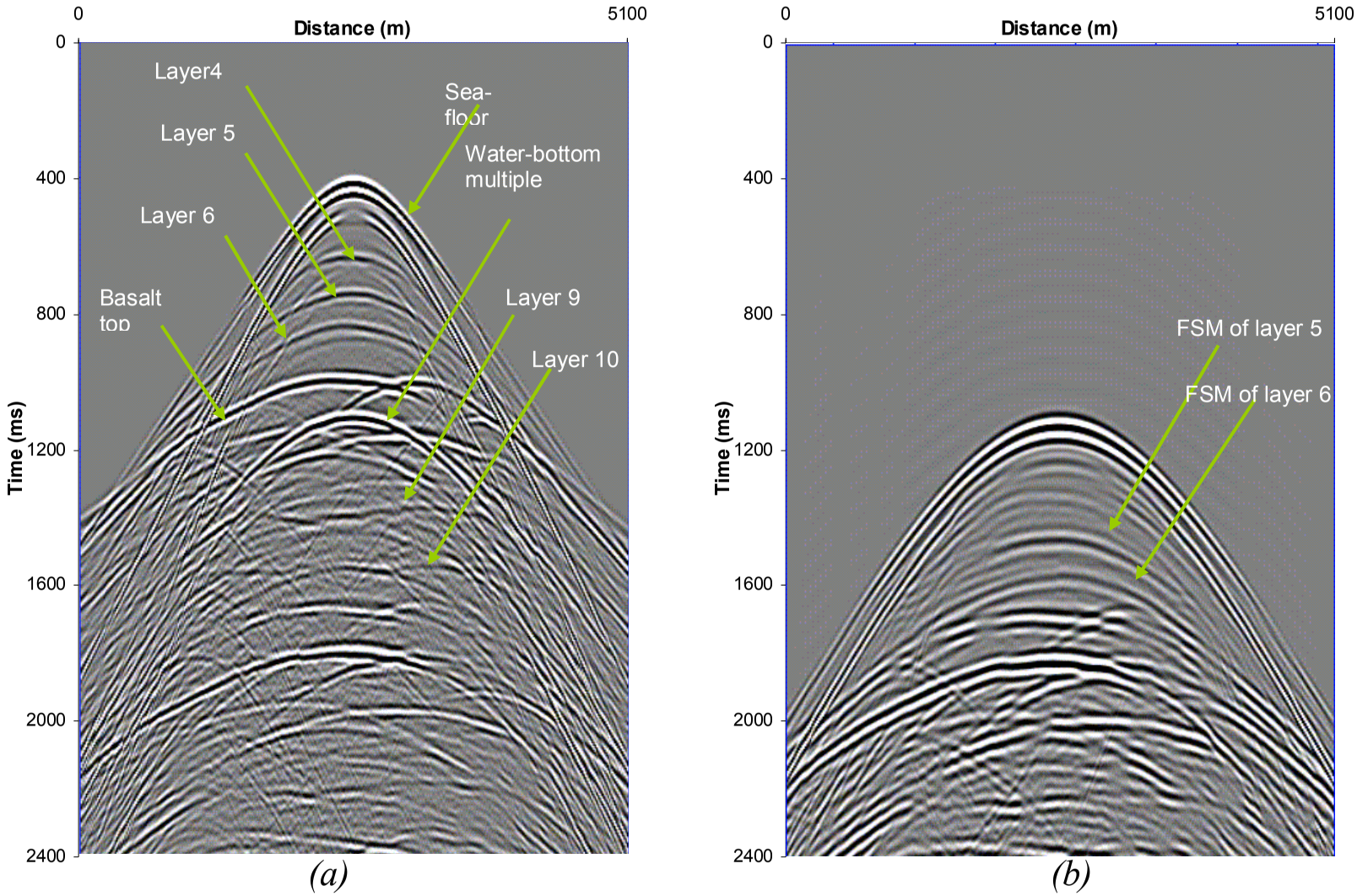

Figure 3.9: (a) Illustration of a shot gather for OBS data. Note that although the sub-basalt layers 9 and 10 are visible they are distorted due to interference from the FSM of the overlying layers 5 and 6 respectively. (b) Illustration of the field of predicted multiples for the OBS data shown in (a). Note that the FSM of layer 5 and 6 arrive at the same time as layer 9 and 10 in (a).

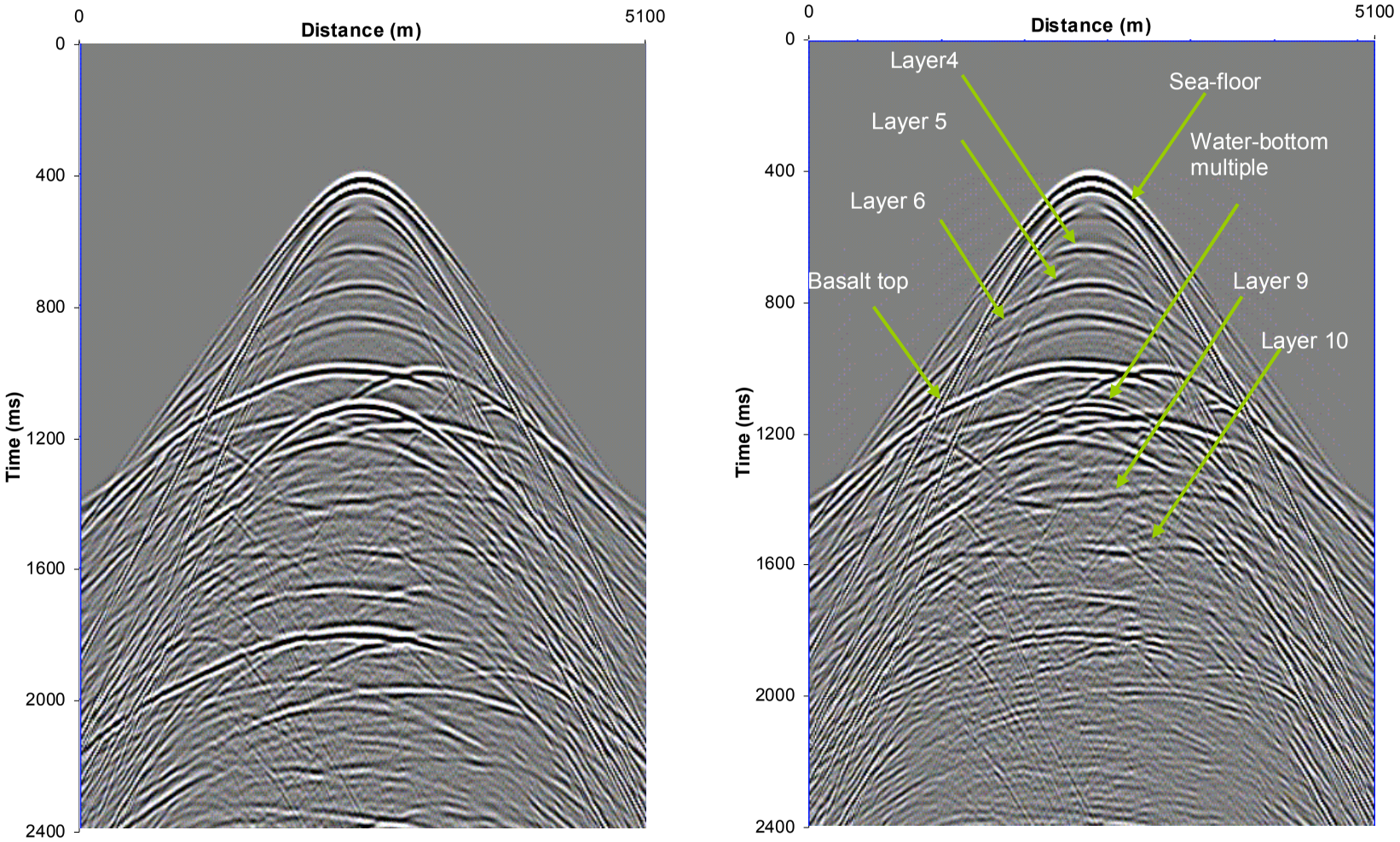

Figure 3.10: Comparison of raw OBS data (a) and demultiple OBS data (b). Note that sub-basalt layers 9 and 10 are clearly visible after demultiple and are more continuous than in the raw data.

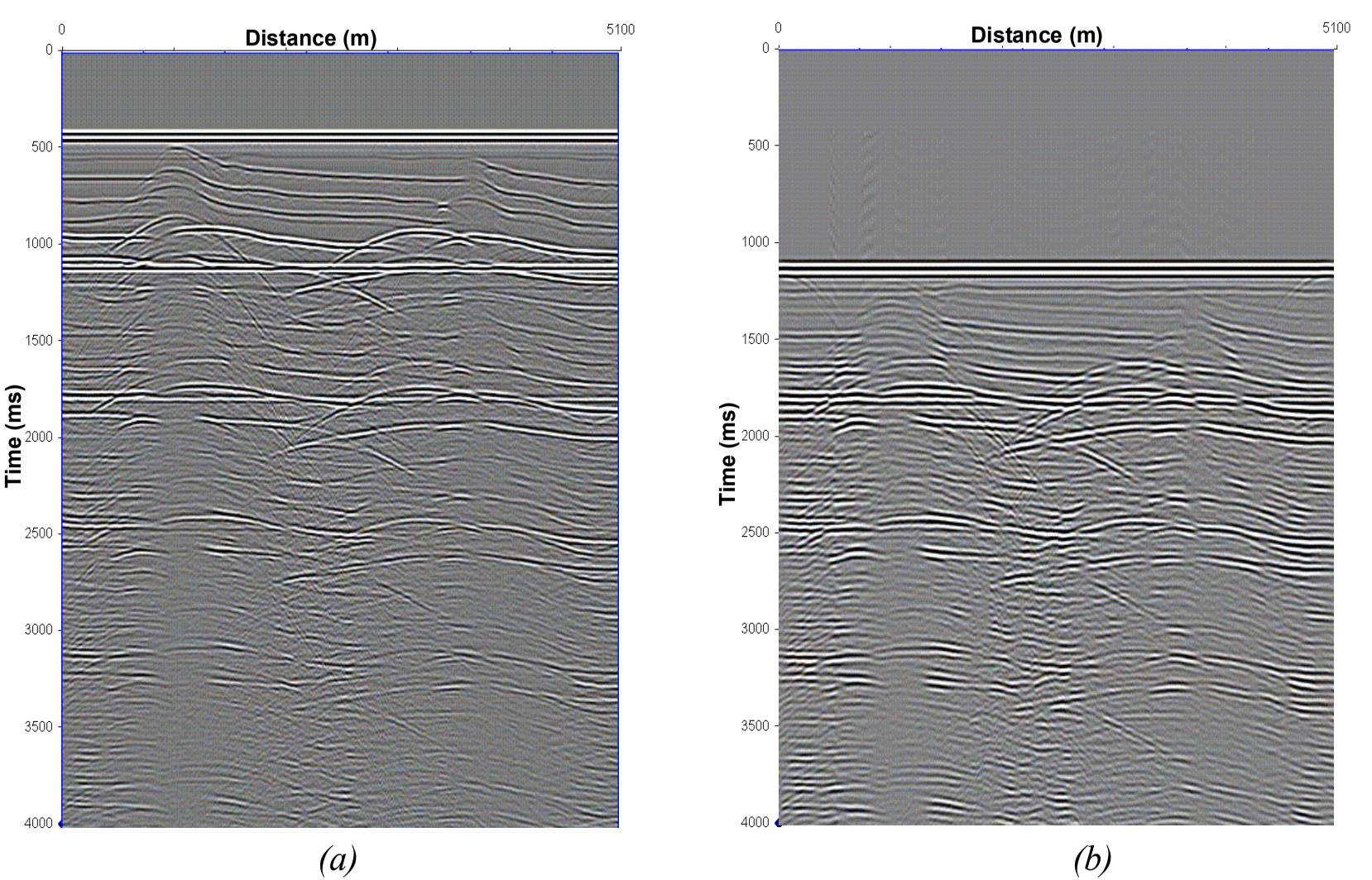

Figure 3.11: A comparison of zero-offset OBS raw data (a) and zero-offset OBS predicted multiples (b). Note that the predicted multiples pick up all the FSM events in the raw data.

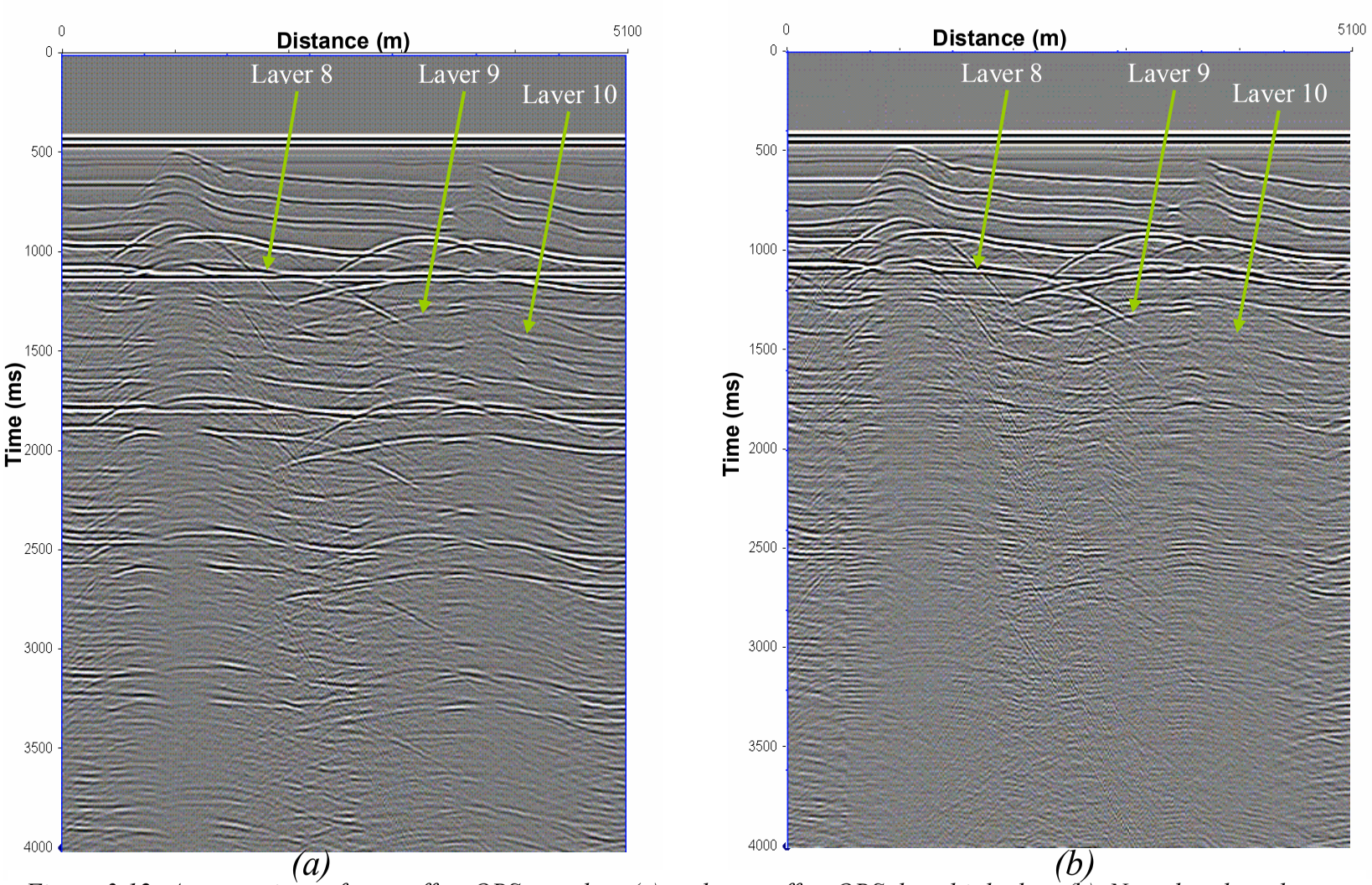

Figure 3.12: A comparison of zero-offset OBS raw data (a) and zero-offset OBS demultiple data (b). Note that the sub-basalt reflectors that were not readily traceable in raw OBS data due to interference with the multiples can be better seen after multiple- attenuation.

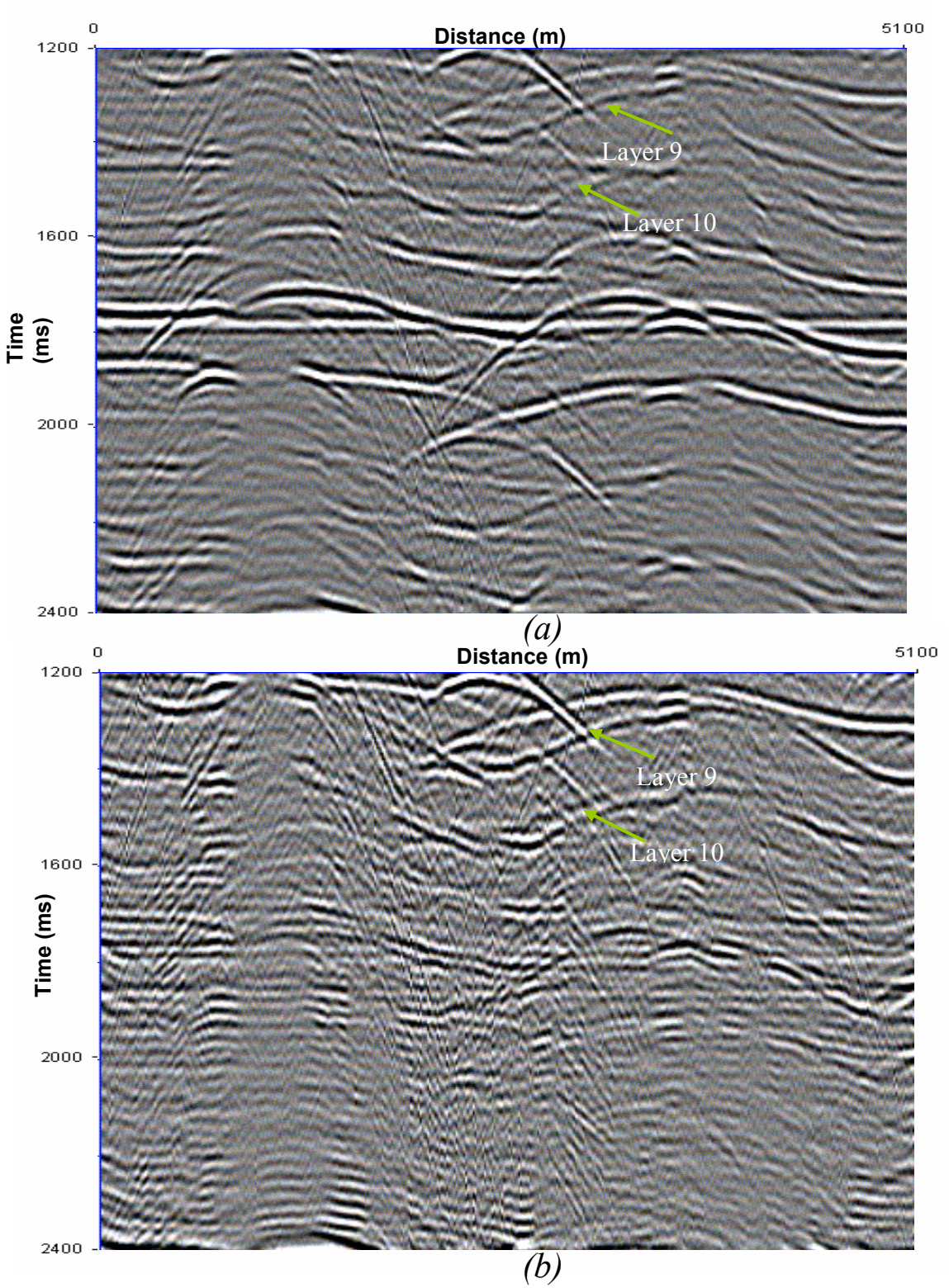

Figure 3.13: A blow-up of Figure 3.12 is shown in this figure from 1200ms to 2400ms. Note that the sub-basalt reflectors from layers 9 and 10 can be easily seen after multiple attenuation.

MODEL II

Due to the rough surface of the basalt, which causes significant scattering of energy, the sub-basalt layers that are visible in Model I are difficult to follow in the raw data for Model II (Figure 3.14a). As we can see in the field of predicted multiples, the multiples pass over the area where sub-basalt layer 10 is expected (Figure 3.14b and Figure 3.15b). A comparison of raw and demultiple data in the shot gathers (Figure 3.16b) as well as zero offset gathers (Figure 3.17a) shows that layers 9 and 10 are drowned in the noise. After demultiple, the layers can be easily traced through the seismic section, although they are not as continuous as they are in Model 1. We have zoomed the zero offset data containing layers 9 and 10 (Figure 3.18) to clearly illustrate the improvement in imaging of the sub-basalt reflectors and to highlight how the continuity of these reflectors has improved.

We conclude that for Model II, the imaging corresponding to this model is possible with the BMG technique of multiple attenuation. Thus this technique will work well in areas having a rough basalt top and bottom. In fact a rough top and bottom is common to almost all volcanic basins, but in particular to the Voring and More basins of Mid-Norway and parts of the West Greenland basins.

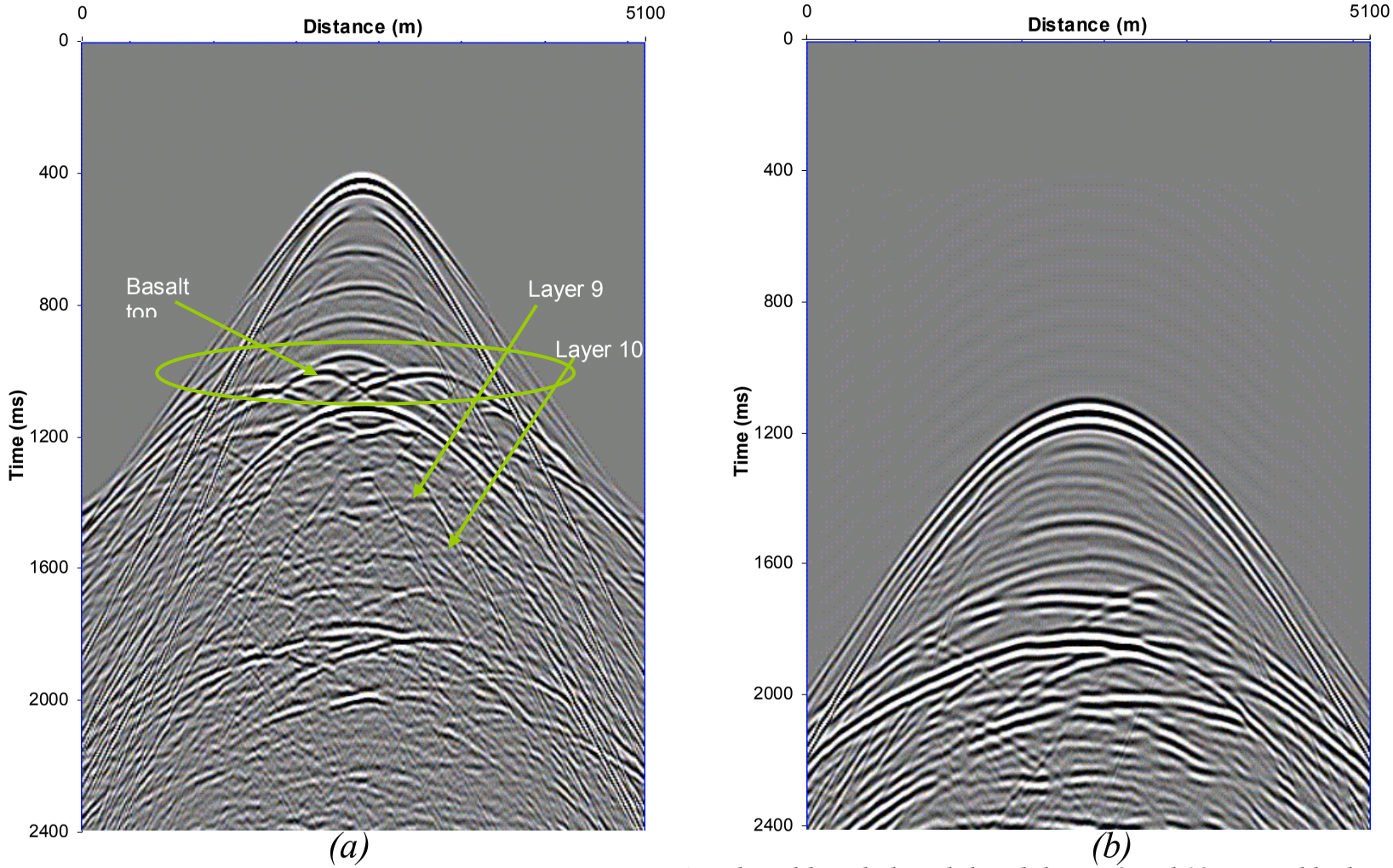

Figure 3.14: (a) Illustration of a shot gather for OBS data. Note that although the sub-basalt layers 9 and 10 are visible they are heavily distorted due to scattering from the basalt and interference from the FSM of the overlying layers 5 and 6 respectively. (b) Illustration of the field of predicted multiples for the OBS data shown in (a). Note that the FSM of layer 5 and 6 arrive at the same time as layer 9 and 10 in (a).

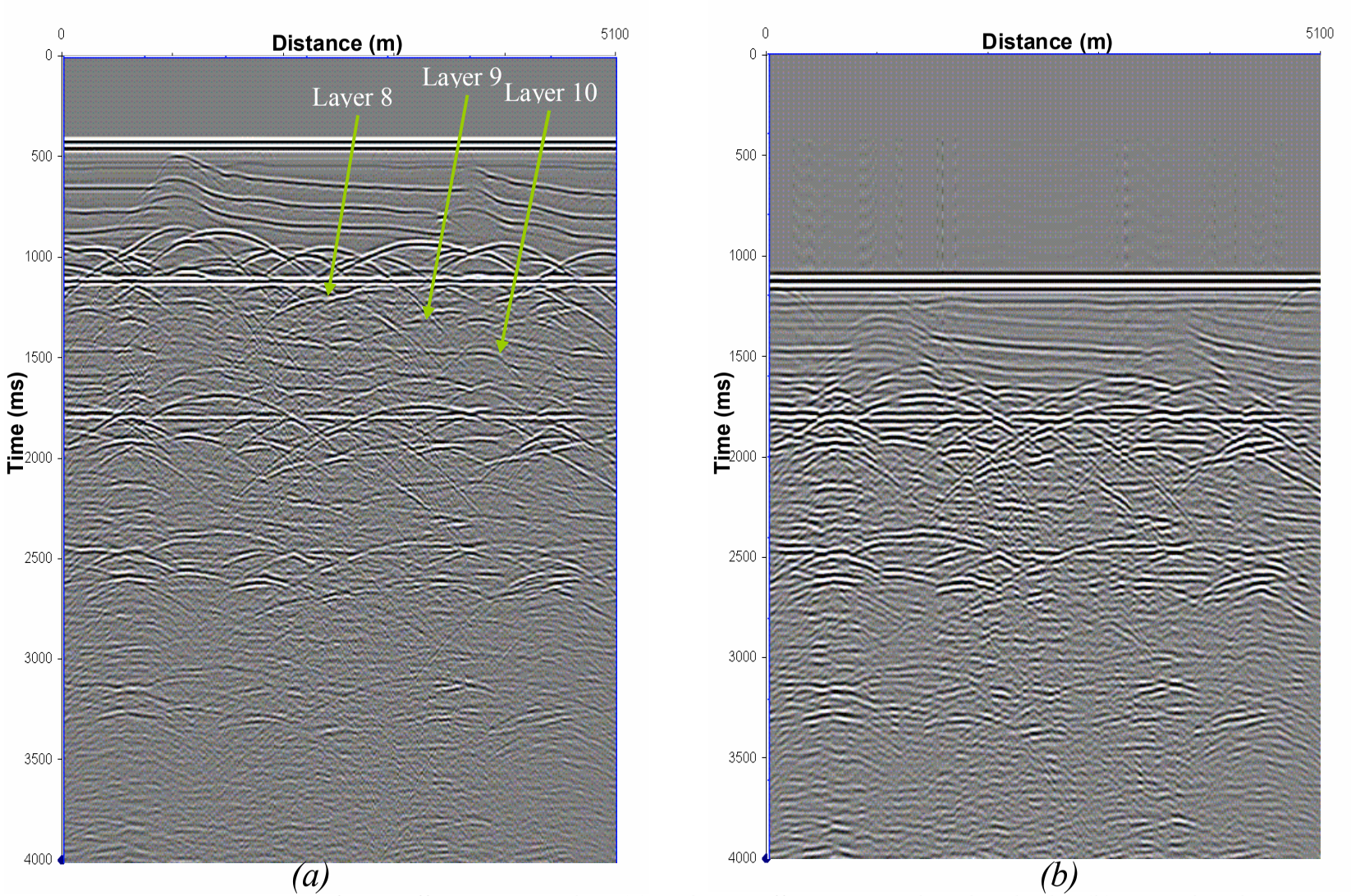

Figure 3.15: A comparison of zero-offset OBS raw data (a) and zero-offset OBS predicted multiples (b). Note that the predicted multiples pick up all the FSM events in the raw data.

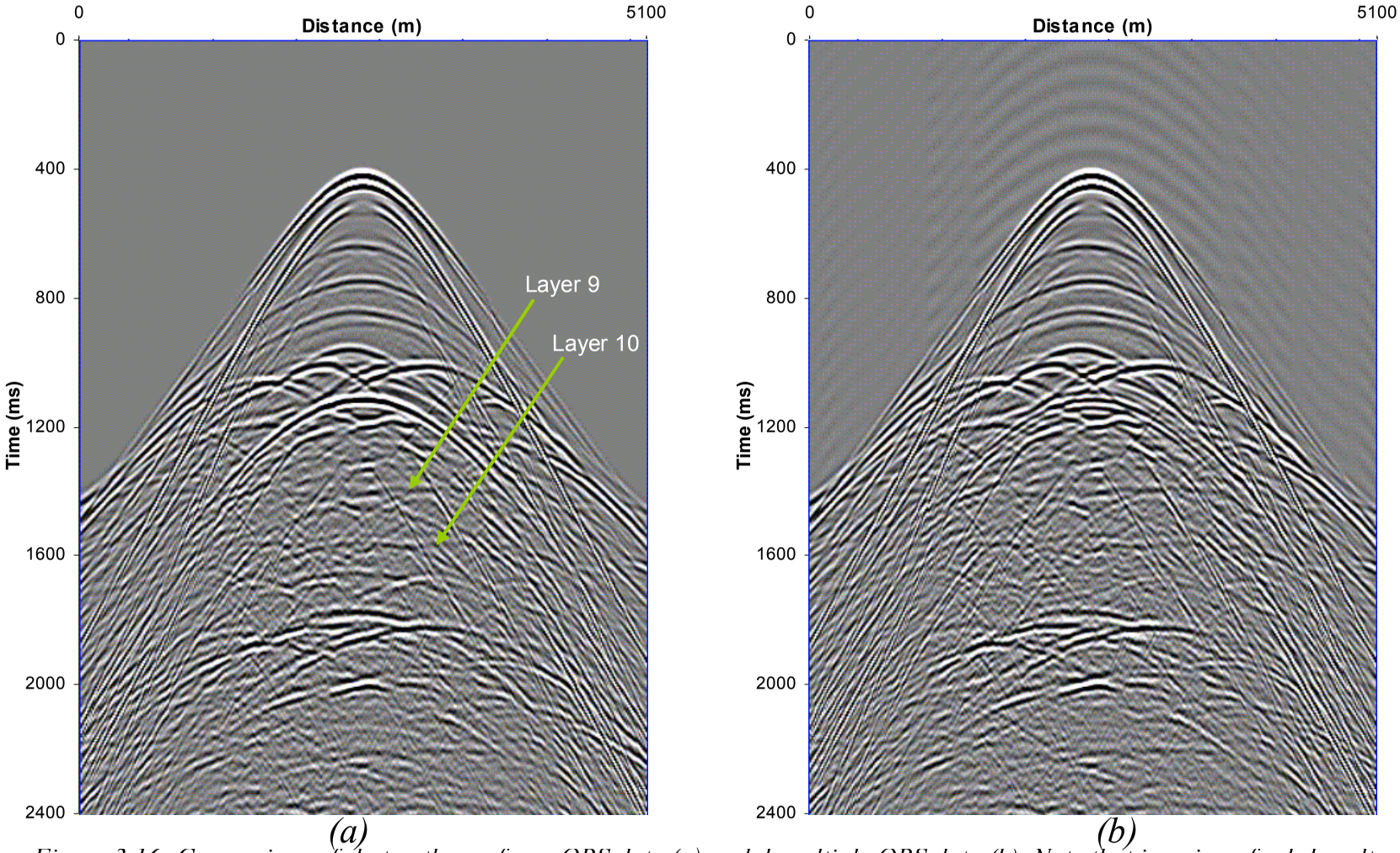

Figure 3.16: Comparison of shot gathers of raw OBS data (a) and demultiple OBS data (b). Note that imaging of sub-basalt layers 9 and 10 has improved due to the attenuation of FSM of the overlying layers although due to distortion it is not as good as in Model I.

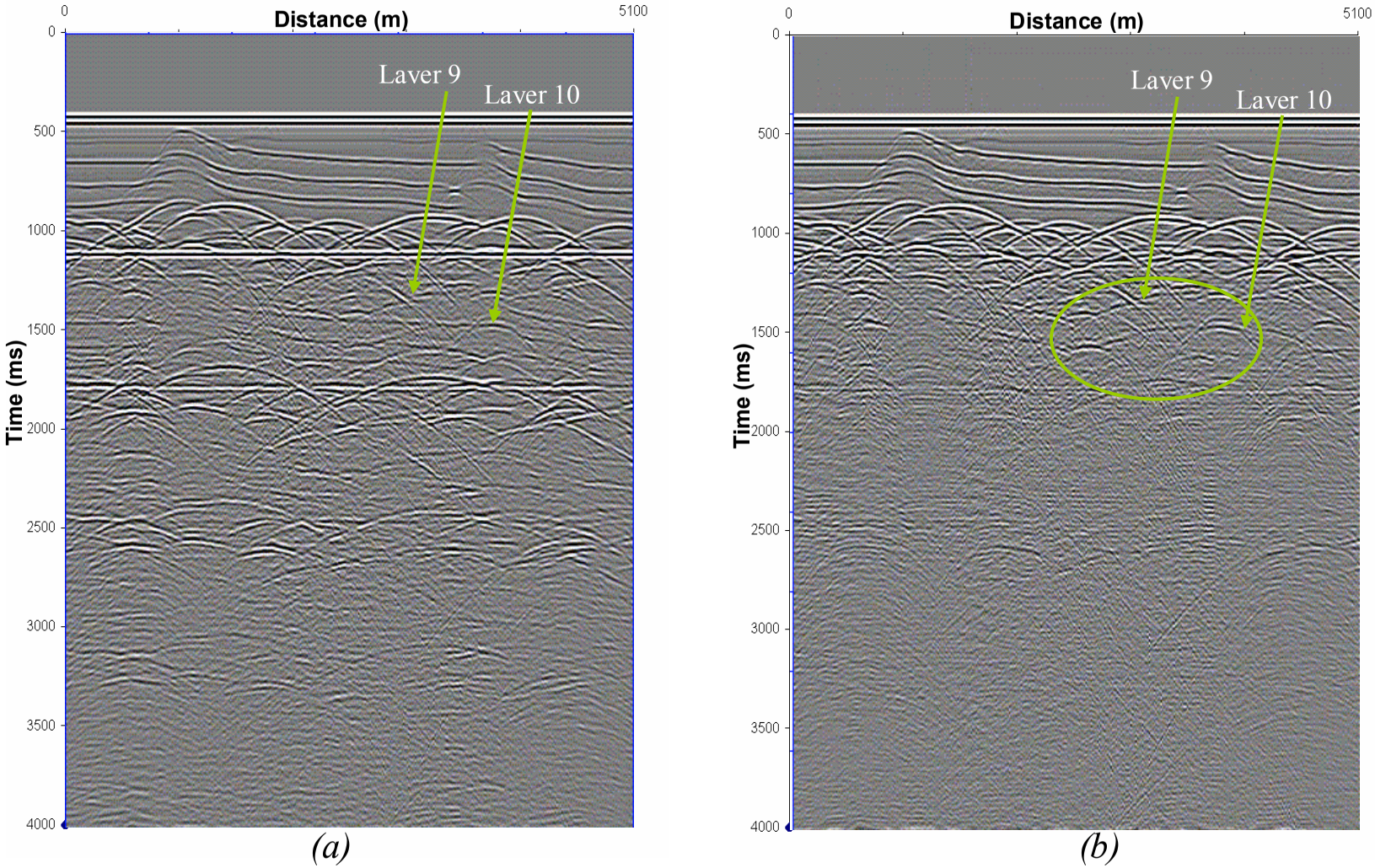

Figure 3.17: A comparison of raw OBS data (a) with demultiple data (b). Note that in Model II also the sub-basalt layers 9 and 10 are visible and are fairly continuous through the seismic section.

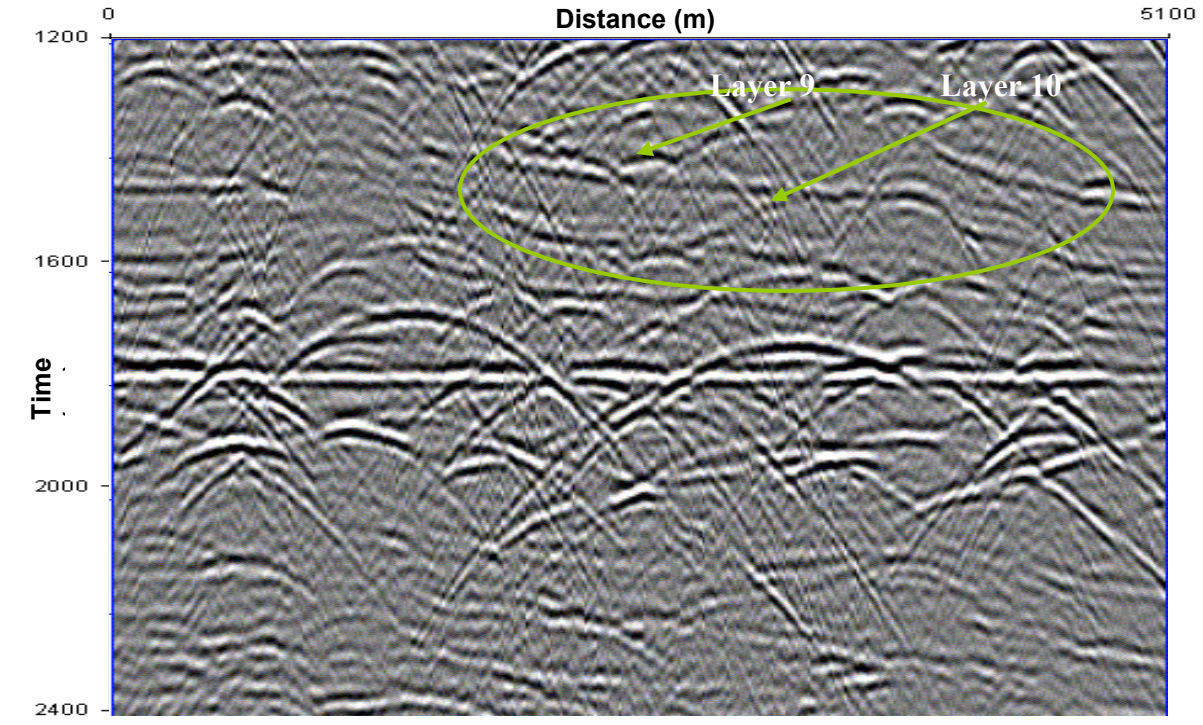

(a)

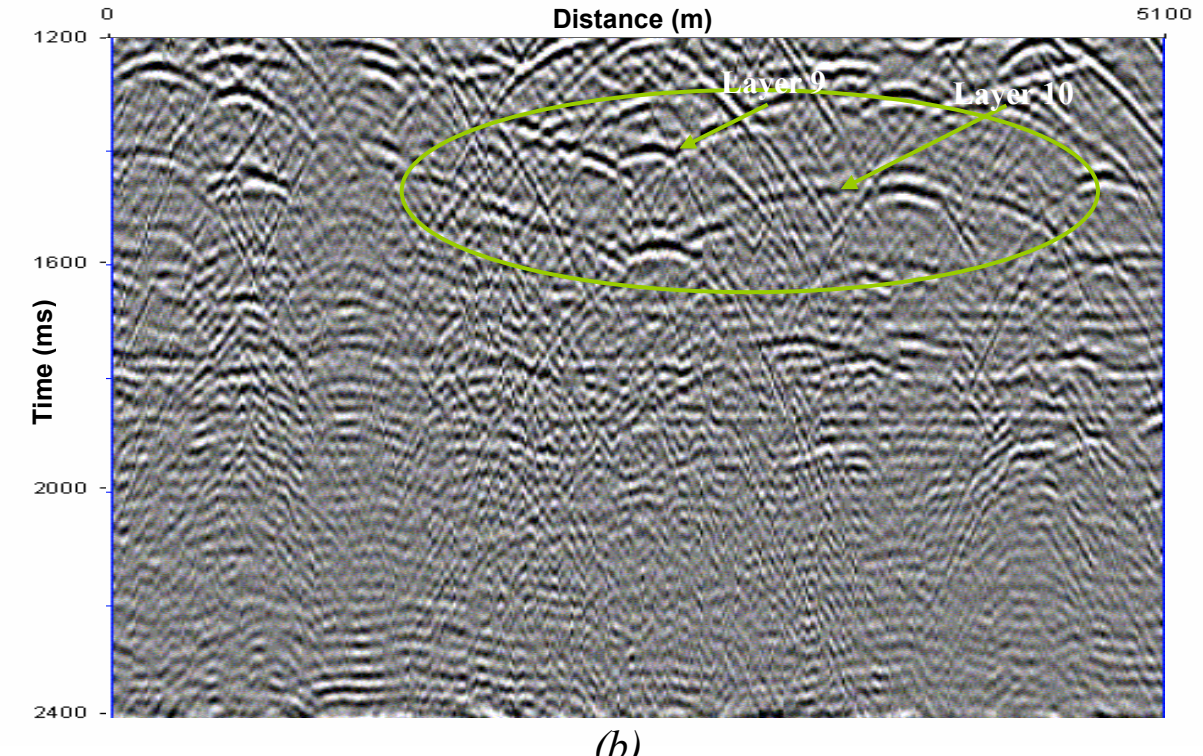

(b)

Figure 3.18: A blow-up of Figure 3.17 is shown in this figure from 1200ms to 2400ms. Note that the sub-basalt reflectors from layers 9 and 10 can be easily seen after multiple attenuation even though they are distorted.

MODEL III

In Model III the effect of intra-bedded units of basalt severely hampers the imaging of sub-basalt layers as they totally obscure the sub-basalt layers by interfering with them (Figure 3.19a).The field of predicted multiples (Figure 3.19b) show that they produce very strong multiples so much so that even the third and fourth-order FSM have significant energy to dominate the seismic picture, as shown in the zero-offset section of predicted multiples in Figure 3.20b.

Demultiple data in Figure 3.21b show very little improvement in signal-to-noise ratio as still significant FSM are present in the data. A comparison of the zero-offset gather for raw OBS data and the demultiple data (Figure 3.22) shows that the method fails to attenuate the FSM in this case, even though Figure 3.23b shows that the multiples are predicted successfully. We recommend that to demultiple data for such volcanic basins we revisit the subtraction scheme described in Appendix B. Basins such as the Deccan Traps of India may not reveal much by the application of the present technique.

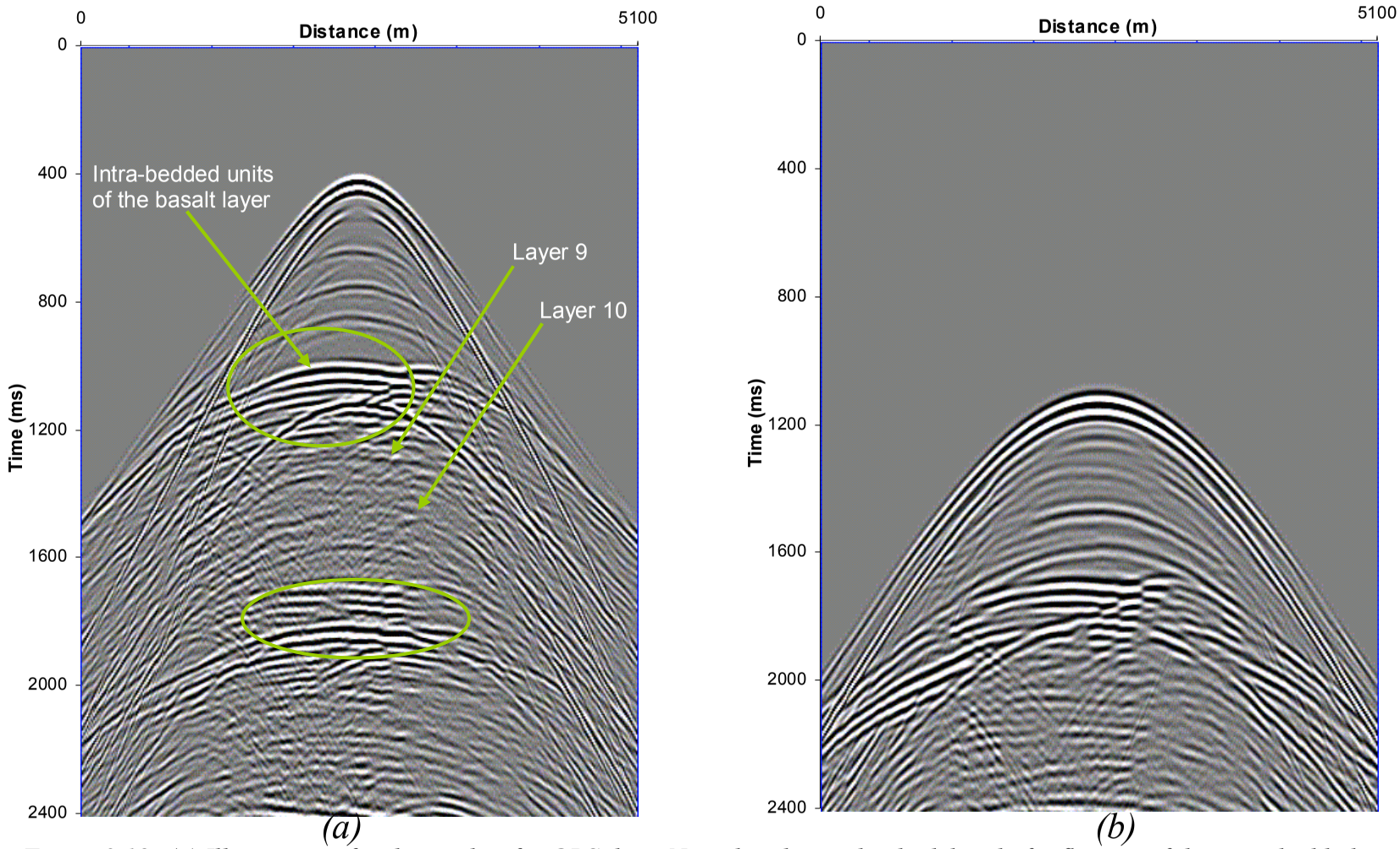

Figure 3.19: (a) Illustration of a shot gather for OBS data. Note that due to the thick band of reflectors of the intra-bedded units of the basalt layer that weakens the energy of the sub-basalt layers as well as distorts them it is difficult to see the sub-basalt layers 9 and 10. Labeling shows where the layers 9 and should be. (b) Illustration of the field of predicted multiples for the OBS data shown in (a). We can see that all the multiples are predicted.

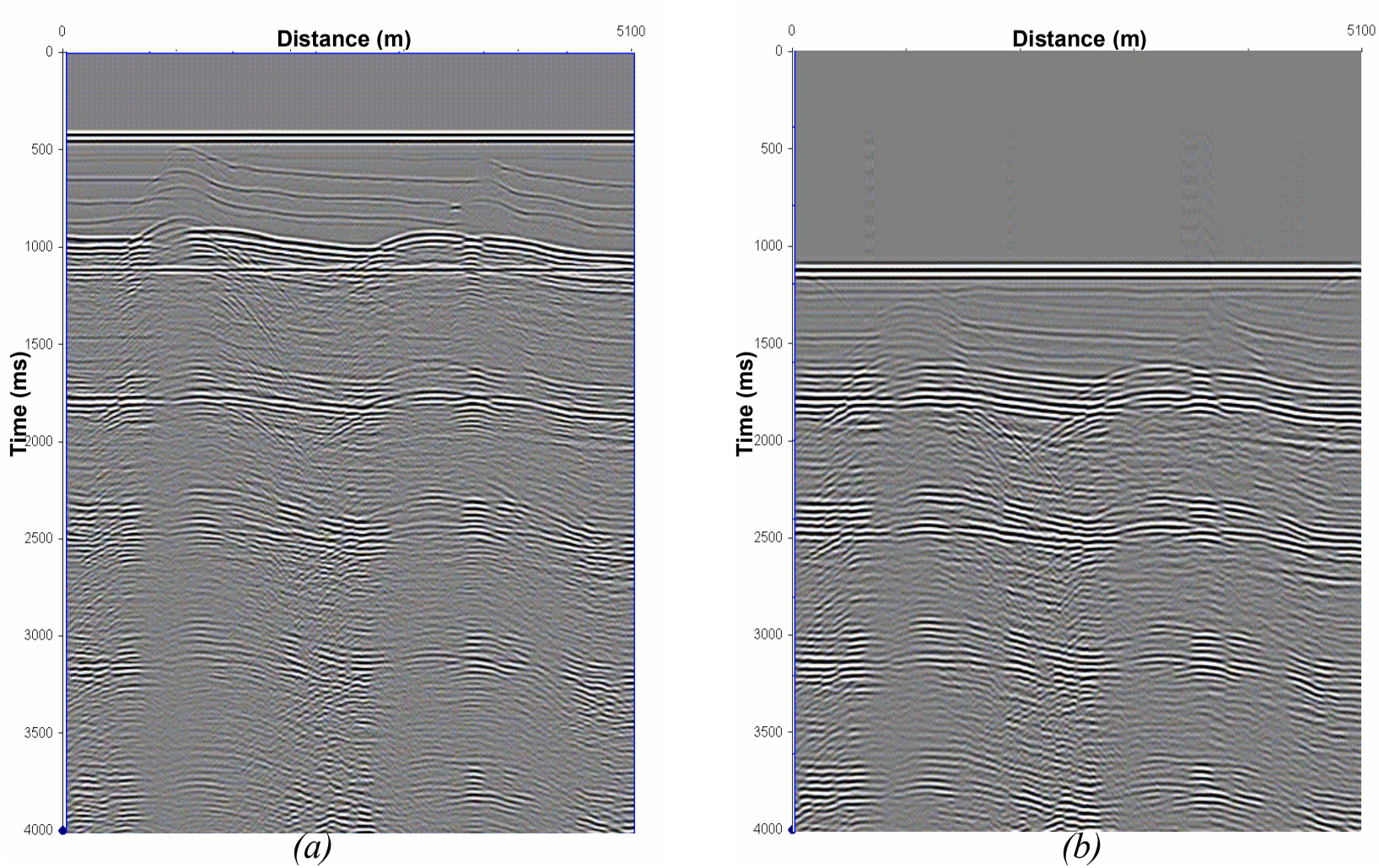

Figure 3.20: A comparison of zero-offset OBS raw data (a) and zero-offset OBS predicted multiples (b). Note that the predicted multiples pick up all the FSM events in the raw data.

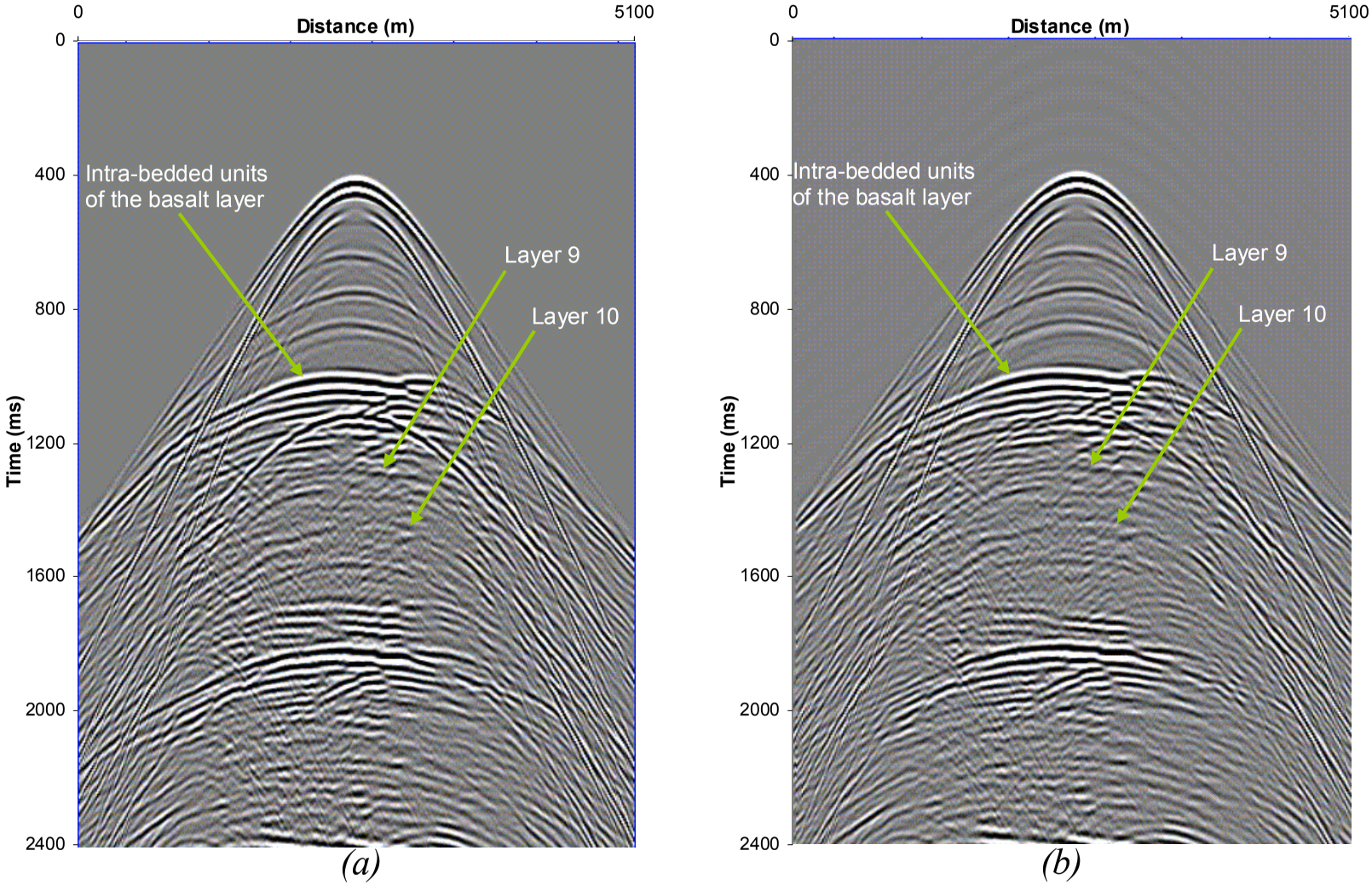

Figure 3.21: Comparison of shot gathers of raw OBS data (a) and demultiple OBS data (b). Note multiple attenuation of data has failed to improve the seismic picture. Layers 9 and 10 are not visible after demultiple of data. The figure shows where the two layers should be.

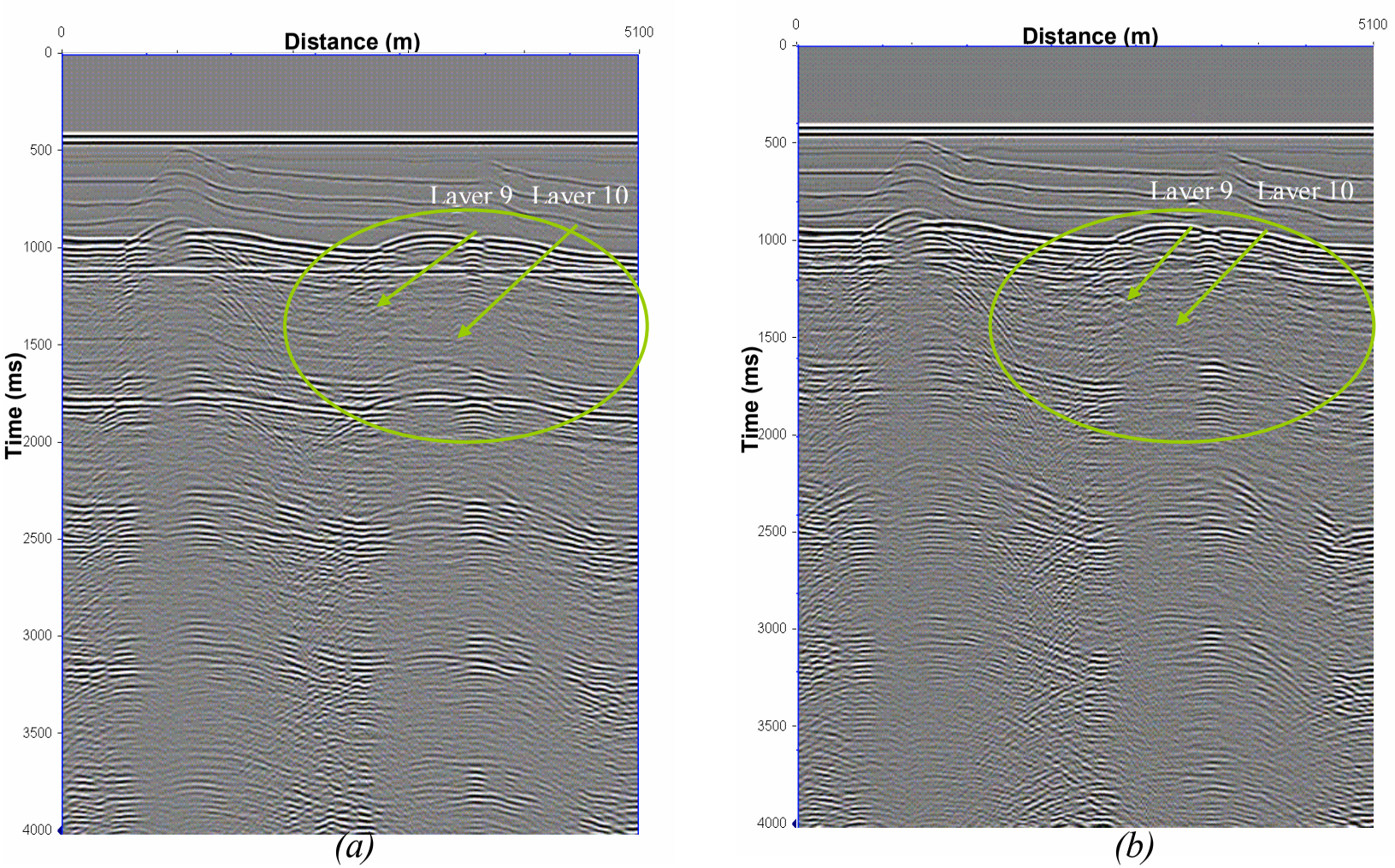

Figure 3.22: Comparison of zero-offset raw OBS data (a) and demultiple OBS data (b). We can see that the multiple attenuation technique fails to attenuate the multiples appreciably in this case . Thus for this case imaging of sub-basalt cannot be warranted.

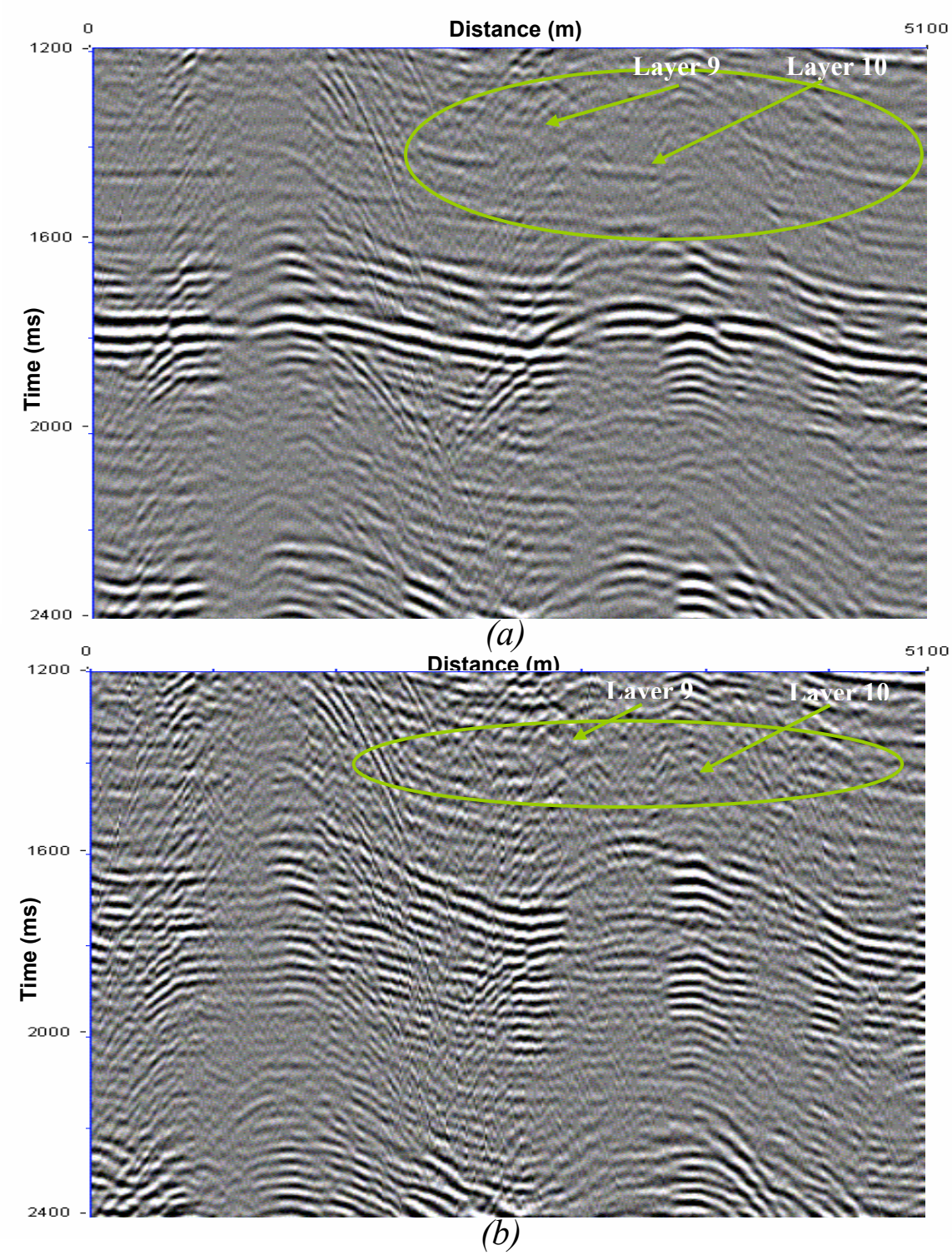

Figure 3.23: A blow-up of Figure 3.20 show that the BMG technique predicts the FSM successfully.

MODEL IV

The small-scale heterogeneities have completely obscured the sub-basalt reflectors, as shown in Figure 3.24a. The distortion of sub-basalt reflections by these heterogeneities has totally hidden the sub-basalt reflections. The shot gather (Figure 3.19) shows that the picture is so distorted that it is difficult to see anything below the basalt layer.

It will be difficult to analyze whether the imaging will be able to reveal the sub-basalt layers. But one thing is clear; the demultiple technique works well for this case. Figure 3.24b and Figure 3.25b show that all the multiples are well predicted while Figure 3.26a and Figure 3.26b show that the FSM have been effectively attenuated. Figure 3.27 shows the zero-offset section for raw OBS data and for demultiple data. It is clear that the demultiple technique successfully attenuates the FSM. However in Figure 3.28 (blow-up of Figure 3.27) shows that it is still not possible to trace the sub-basalt reflections after successful demultiple.

Hence we can conclude that although the demultiple technique works well for Model IV and helps in attenuating the FSM, a successful migration of such data cannot be warranted. Places like the Northwest. Australian basins and the Karoo basins are known to have such heterogeneities.

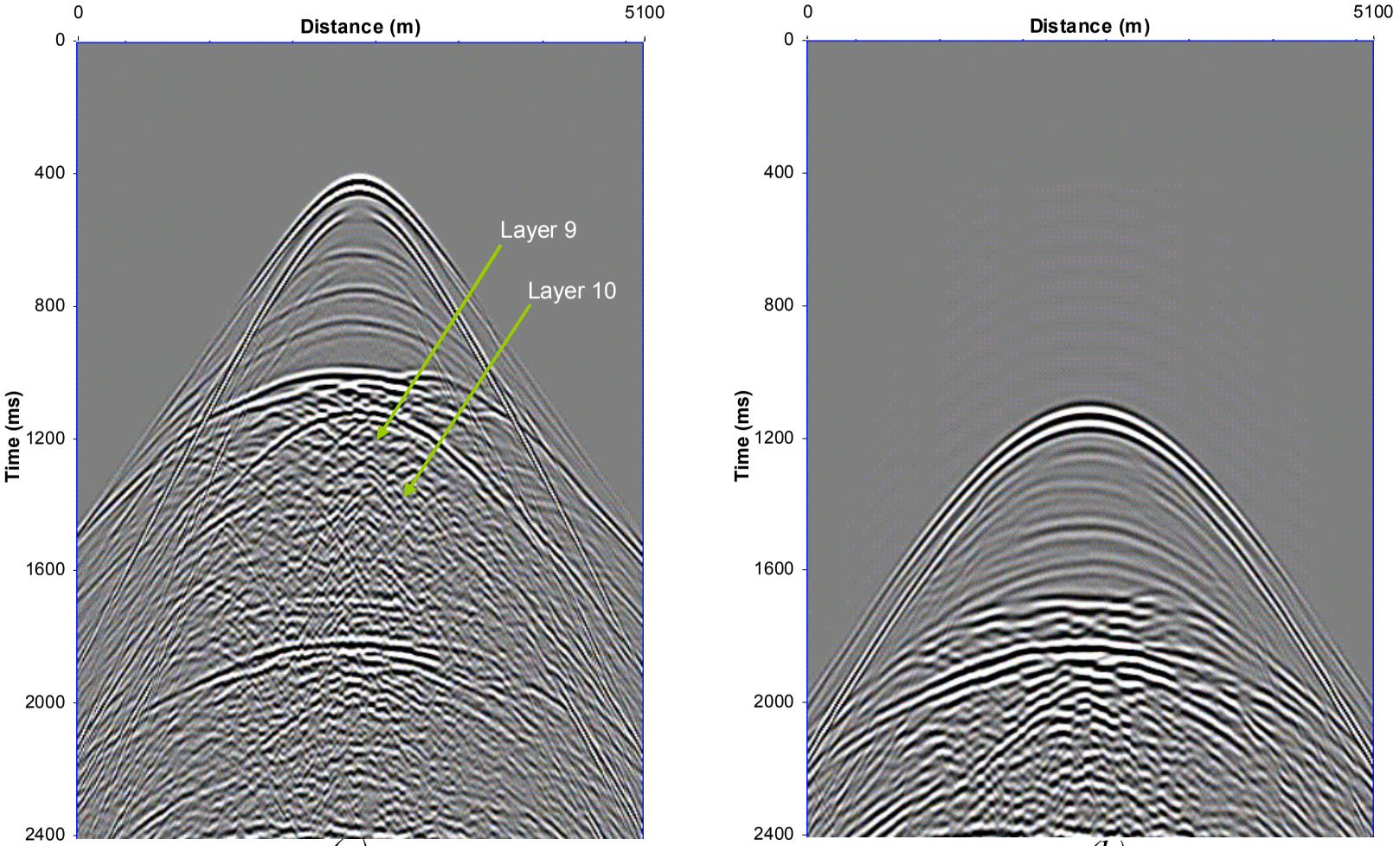

Figure 3.24: (a) Illustration of a shot gather for OBS data. Note that due to the small-scale heterogeneities in the basalt layer the events below the basalt layers are very distorted making it difficult to see the sub-basalt layers 9 and 10. Labeling shows where the layers 9 and should be. (b) Illustration of the field of predicted multiples for the OBS data shown in (a).

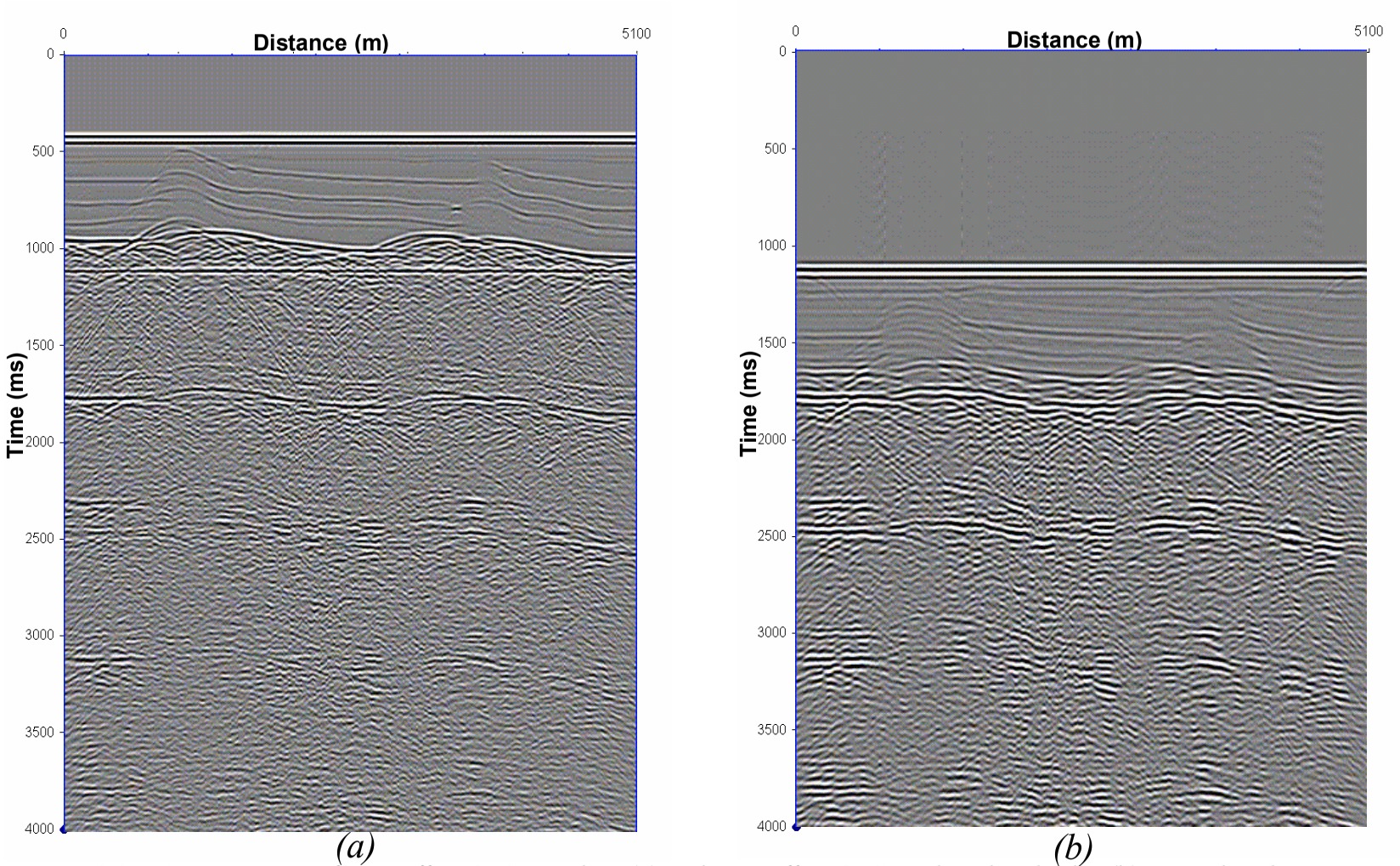

Figure 3.25: A comparison of zero-offset OBS raw data (a) and zero-offset OBS predicted multiples (b). Note that the predicted multiples pick up all the FSM events in the raw data.

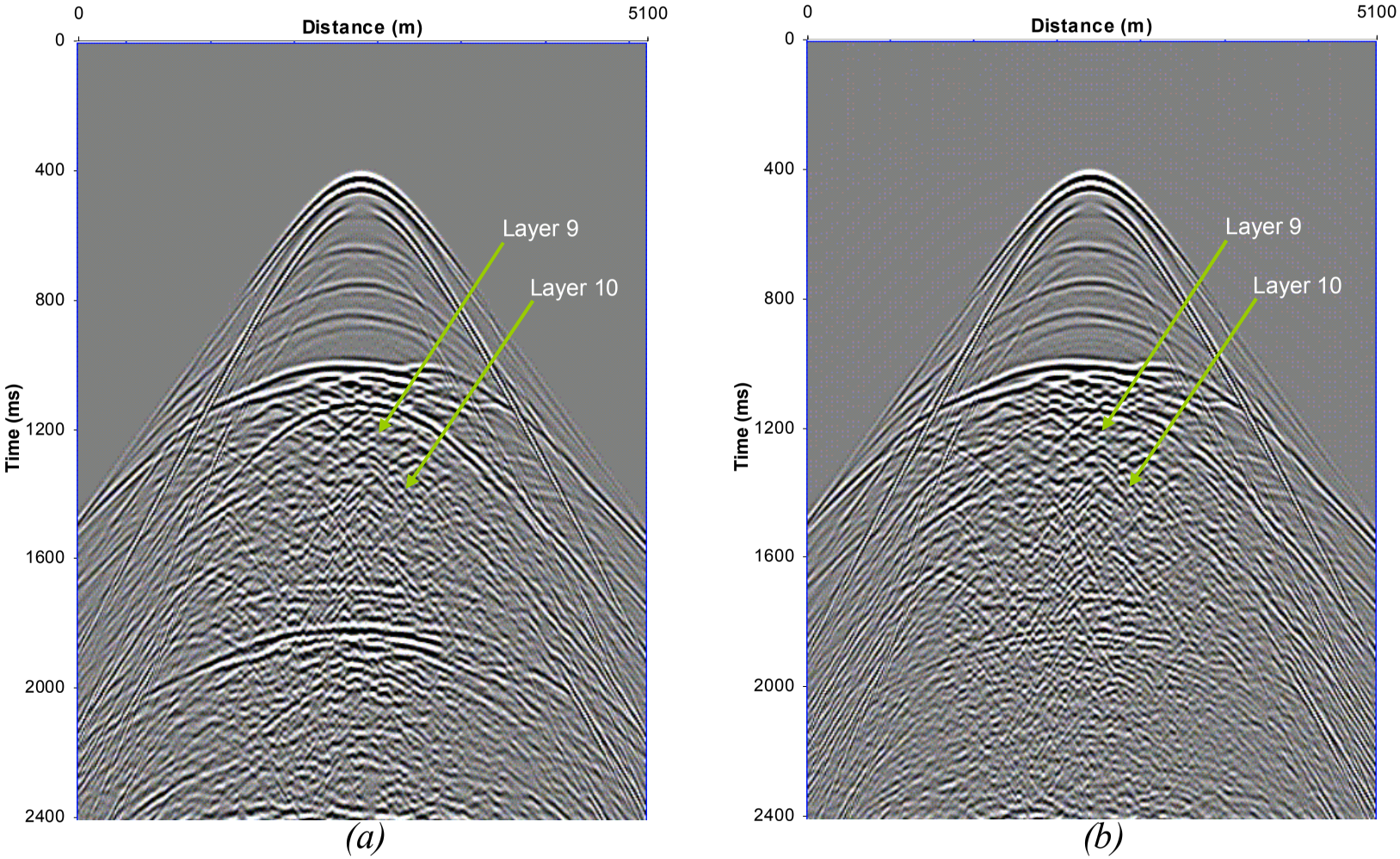

Figure 3.26 Comparison of raw OBS data (a) and demultiple OBS data (b). Even though the multiple attenuation technique works successfully on this data due to distortion of the sub-basalt layers 9 and 10 by the small scale heterogeneities in the basalt layer, they cannot be imaged.

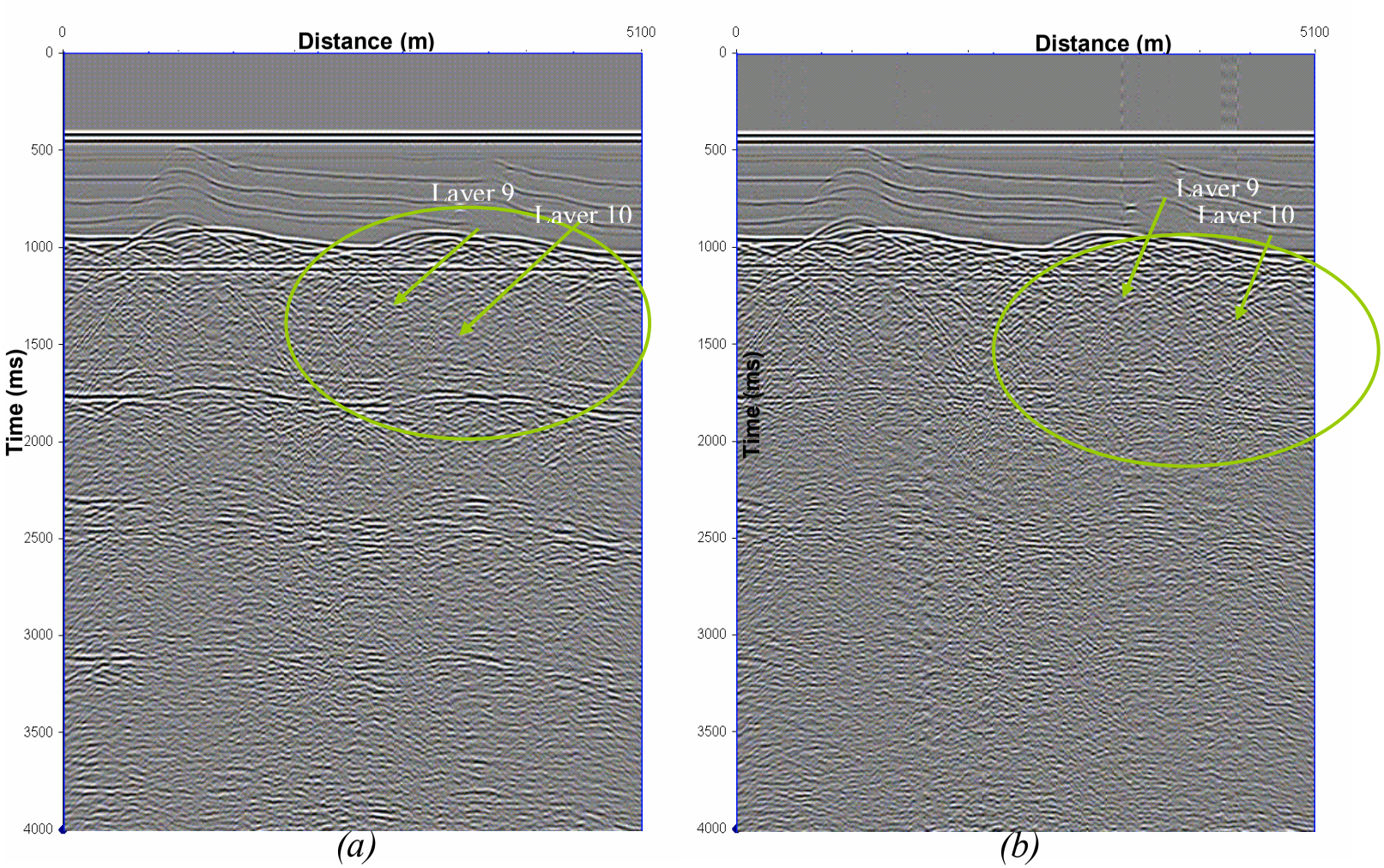

Figure 3.27: A comparison of zero offset raw OBS data (a) with the demultiple OBS data (b). The demultiple technique for this case has attenuated the multiples appreciably making the shot gather a lot cleaner. Note that the sub-basalt layers 9 and 10 are still not visible but that is due to scattering of energy from the small-scale heterogeneities in the basalt.

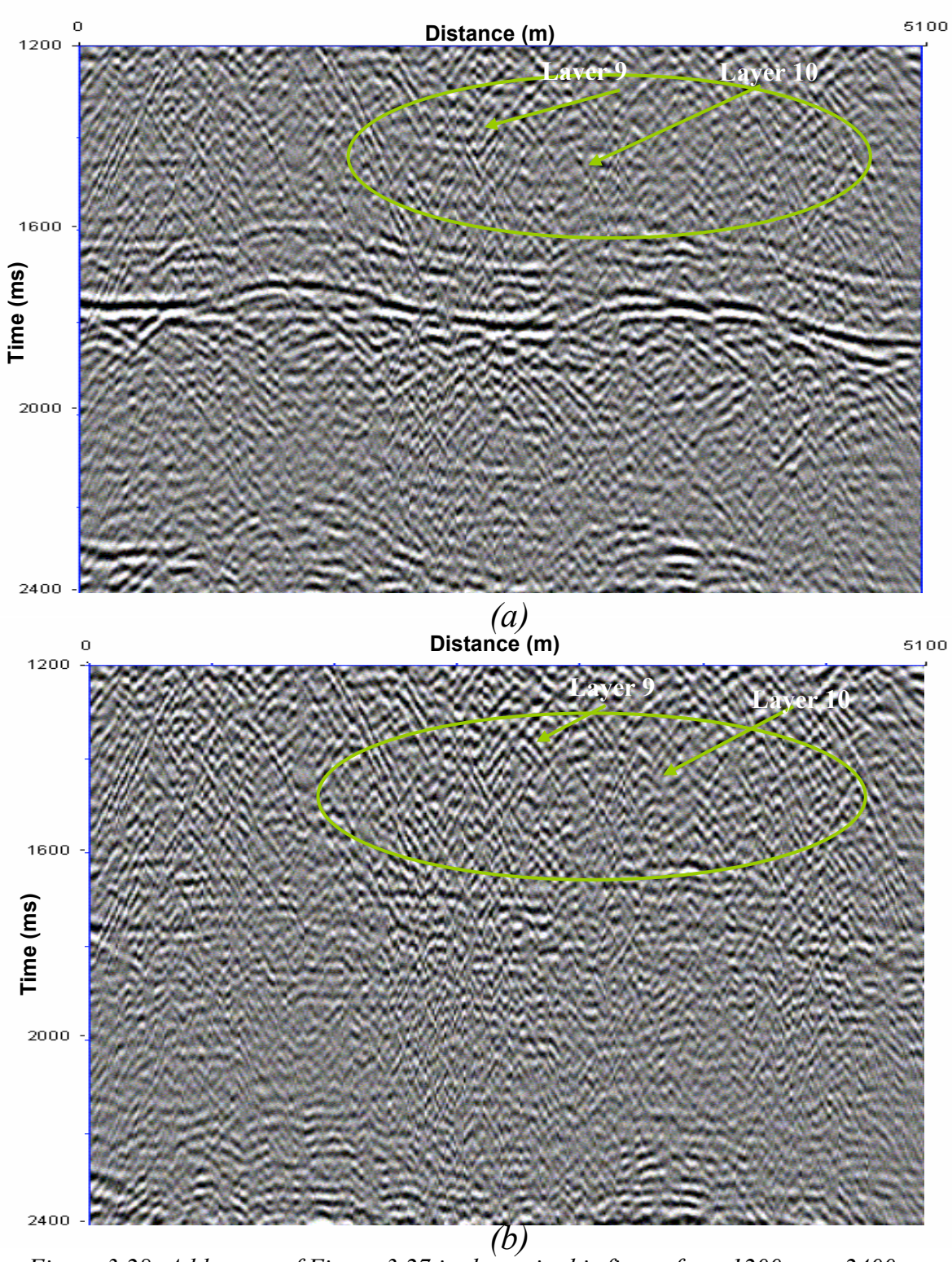

Figure 3.28: A blow-up of Figure 3.27 is shown in this figure from 1200ms to 2400ms. Note that the multiple technique works very well for this technique. Layers 9 and 10, which are not visible in raw data due to distortion from the basalt layer, are still not visible.

CHAPTER IV

SUMMARY AND CONCLUSIONS

For imaging the sub-basalt layers, we have proposed a way of modeling the complexities of the basalt layer into just four categories that incorporate all known complexities in basalt deposits known around the world. We propose that simplifying the models by categorizing them into four categories and studying the effect of each category separately will give us an insight into how each complexity respond to a particular processing step. This will not only help in simplifying the study of complex volcanic basins and help in finding the right processing steps and parameters to use in imaging of sub-basalt reflections, but also give us some idea of what kind of heterogeneities are present in the basin.

We also adapted the demultiple approach proposed by Ikelle and Amundsen (2004) for application to OBS data and demonstrated that it can be successfully applied to deep-water OBS data.

More specifically, we applied the BMG technique for multiple attenuation and found that the technique effectively works for Models I, II and IV. It is not so effective in Model III even though the technique predicts the multiples of the intra-bedded reflections, as the estimation of the scaling factor for subtraction of predicted multiples is not accurate. This leaves significant residuals in the demultiple data. The result of

demultiple of the various sub-basalt models proposed in this thesis are also summarized in Table 4.1.

Table 4.1: An illustration of applicability of BMG technique in imaging the sub-basalt reflections for the proposed four models.

Processing Technique / Proposed models	BMG (Predict and then Subtract) technique
Model 1	Works well in imaging sub-basalt reflection for basins having relatively smooth basalt surfaces, such as Angola basin
Model 2	Successfully improves imaging of sub-basalt reflections for models having rough basalt top and bottom, e.g. Voring and More basins of Mid-Norway and parts of the West Greenland basins
Model 3	Not successful in imaging the sub-basalt reflections for models having intra-bedded layers in basalt, e.g. Deccan Traps of India.
Model 4	Works well in attenuating the multiples for basins such as Northwest Australian basins and the Karoo basins, but imaging of sub-basalt reflections not guaranteed.

REFERENCES

Barton, P., and Barker, N., 2003, Velocity imaging by tau−p transformation of refracted seismic traveltimes: Geophysical Prospecting, **51**, 195-203.

Bayliss, A., Jordan, R. E., LeMesurier, B. J., and Turkel, E., 1986 A fourth order accurate finite-difference scheme for computation of elastic seismic waves. Bulletin of Seismological Society of America, **76**, 1115-1132.

Fliedner, M. M., and White, R.S., 1999. Using wide-angle seismic data for basalt and sub-basalt imaging. 69th SEG Meeting, Houston, Expanded Abstracts, 1021-1024.

Fliedner, M. M., and White, R. S., 2001, Sub-basalt imaging in the Faeroe-Shetland Basin with large-offset data, First Break, **19** (5), 247-252.

Graves, R. W., 1996, Simulating seismic wave propagation in 3D elastic media using staggered-grid finite differences: Bulletin of Seismological Society of America, **86**, 1091-1106.

Ikelle, L. T., Roberts, G., and Weglein, A. B., 1997, Source signature estimation based on the removal of first-order multiples: Geophysics, **62**, 1904-1920.

Ikelle, L.T., and Amundsen, L., 2002, Non-iterative multiple attenuation methods: Linear inverse solutions to nonlinear inverse problems: The Leading Edge, **21**, 350-356.

Ikelle, L.T., and Amundsen, L., 2003, Introduction to petroleum seismology: Society of Exploration Geophysicists, Tulsa, OK, .

Ikelle, L.T., and Amundsen, L., 2004, Attenuation of primaries and free-surface multiples of towed-streamer data while preserving ghosts of primaries: a linear approach: Journal of Seismic Exploration **13**, 1-15.

Ikelle, L.T., Osen A., Amundsen, and L., Shen Y., 2004, Non-iterative multiple attenuation methods: Linear inverse solutions to non-linear inverse problems – II BMG Approximation, Geophysical Journal International, **159,** 923-930

Planke, S. and Haugen, G. U., 2001, Seismic imaging and interpretation of volcanic constructions. Volcanic Basin Petroleum Research, Statoil, Oslo, Norway.

Watts, A., 2005, Linear Demultiple Solution Based on Bottom-Multiple Generator (BMG) Reflector Approximation: Subsalt Example: Thesis, Texas A&M University, College Station, Texas

White, R. S., Smallwood, J. R., Fliedner, M. M., Boslaugh, B., Maresh, J. and Fruehn, J., 2003, Imaging and regional distribution of basalt flows in the Faeroe-Shetland Basin: Geophysical Prospecting, **51**, 215-232.

Ziolkowski, A., Hanssen, P., Gatliff, R., Jakubowicz, H., Dobson, A., Hampson, G., Li, X.Y., and Liu E., 2003, Use of low frequencies for sub-basalt imaging: Geophysical Prospecting, **51**, 169-182.

APPENDIX A

CONSTRUCTION OF FREE-SURFACE MULTIPLES

Let us discuss the theory of predicting the FSM before we discuss the BMG approach. Ikelle and Amundsen (2002) showed that each seismic event could be decomposed into two or more events at the scattering points or the reflection points (Figure A.1). Conversely, two seismic events can be joined at the scattering point to construct another seismic event. These scattering points can be either at the free surface or in the subsurface. If these scattering points are at the free surface, then only ghosts and FSM can be constructed (Figure A.2). Since we are not considering the ghosts as separate events (as discussed in Chapter I), we can say that only FSM can be predicted if the scattering point is at the free surface (Ikelle and Amundsen 2004). If we look at the raypaths closely, we notice that it is possible to predict only FSM (and ghosts) from the existing events in the data as only these events hit the free surface. If the scattering points are at the water bottom or in the subsurface then primaries and internal multiples can also be constructed. Convolution is the connecting operator used for construction of these events.

Some important inferences that can be drawn from the Figure A.1 and A.2 are as follows:

- No primary can be constructed with the connecting point at the free surface (Figure A.1).
- We can construct ghosts of primaries only if the data contain direct waves. If direct waves are removed from the data then no ghosts of primaries can be predicted.
- First order FSM can be constructed by combining two primaries at one scattering point (Figure A.2). Also, the first-order FSM can be constructed using only one scattering point.
- Second-order free-surface multiples can be constructed by combining primaries and first-order FSM. Note that since the second-order FSM reflect from the free surface twice (Figure A.2), then using one scattering point at the free surface, there are two ways of constructing them by combining primaries and first-order FSM. The second-order FSM can also be constructed using three primaries having two scattering points at the free surface. Thus there are two possible ways of constructing second order FSM with one scattering point at the free surface, and only one way by using two scattering points at the free surface.
- Third-order FSM can be constructed either by a combination of two first-order FSM or by a combination of primary and second-order FSM. There are three possible ways of constructing third-order FSM with one scattering point at the free surface, two possible ways by using two scattering points at the free surface, and one way by using three scattering points at the free surface.

Thus by applying the scattering point at the free surface only and using data free of direct waves, we can predict only the FSM and subtract them from the data.

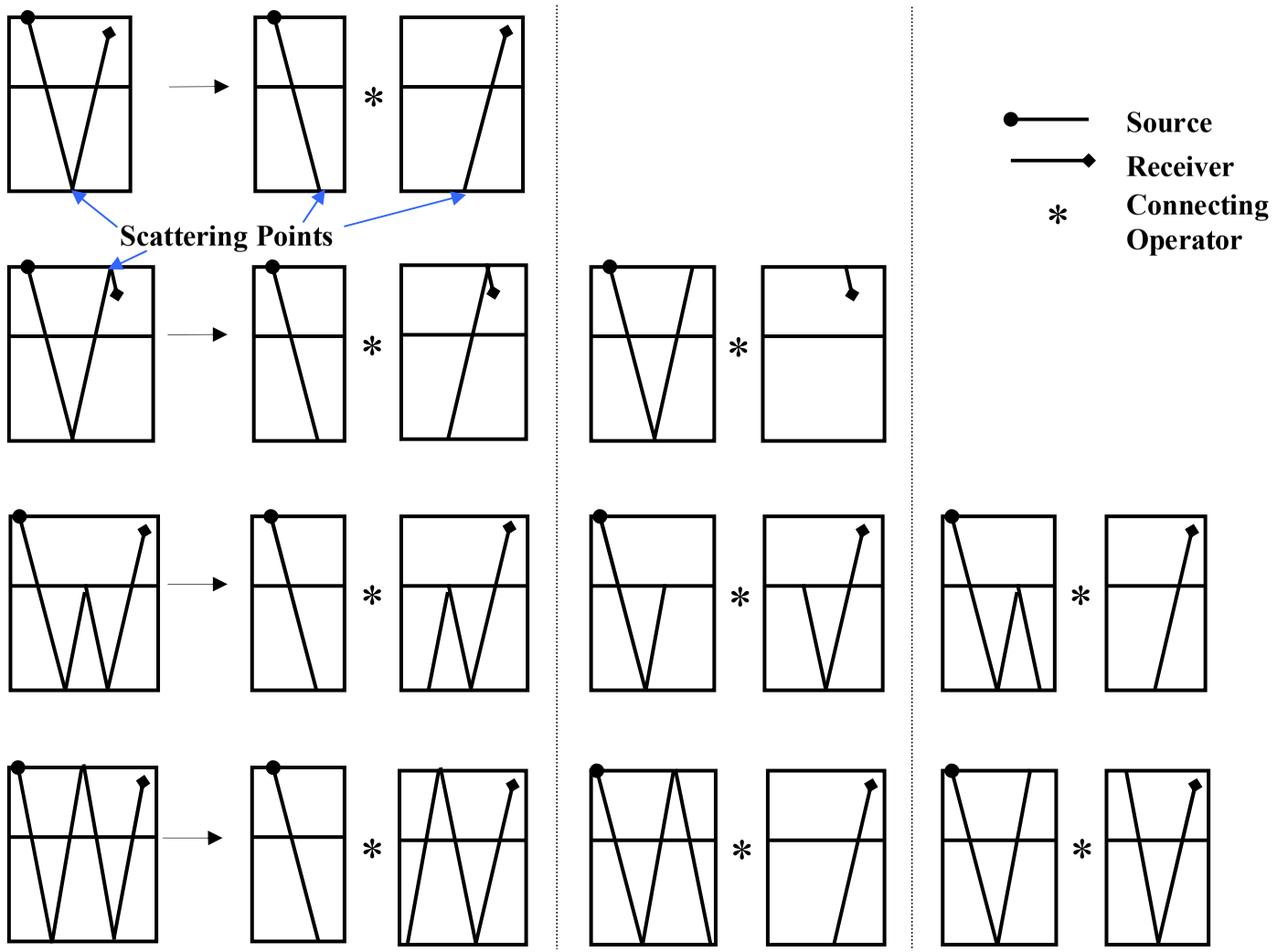

Figure A.1: Illustration of construction of seismic events. This figure shows the case for towed-streamer data. Note that for constructing the primaries and internal multiples we need to have the scattering point in the subsurface.

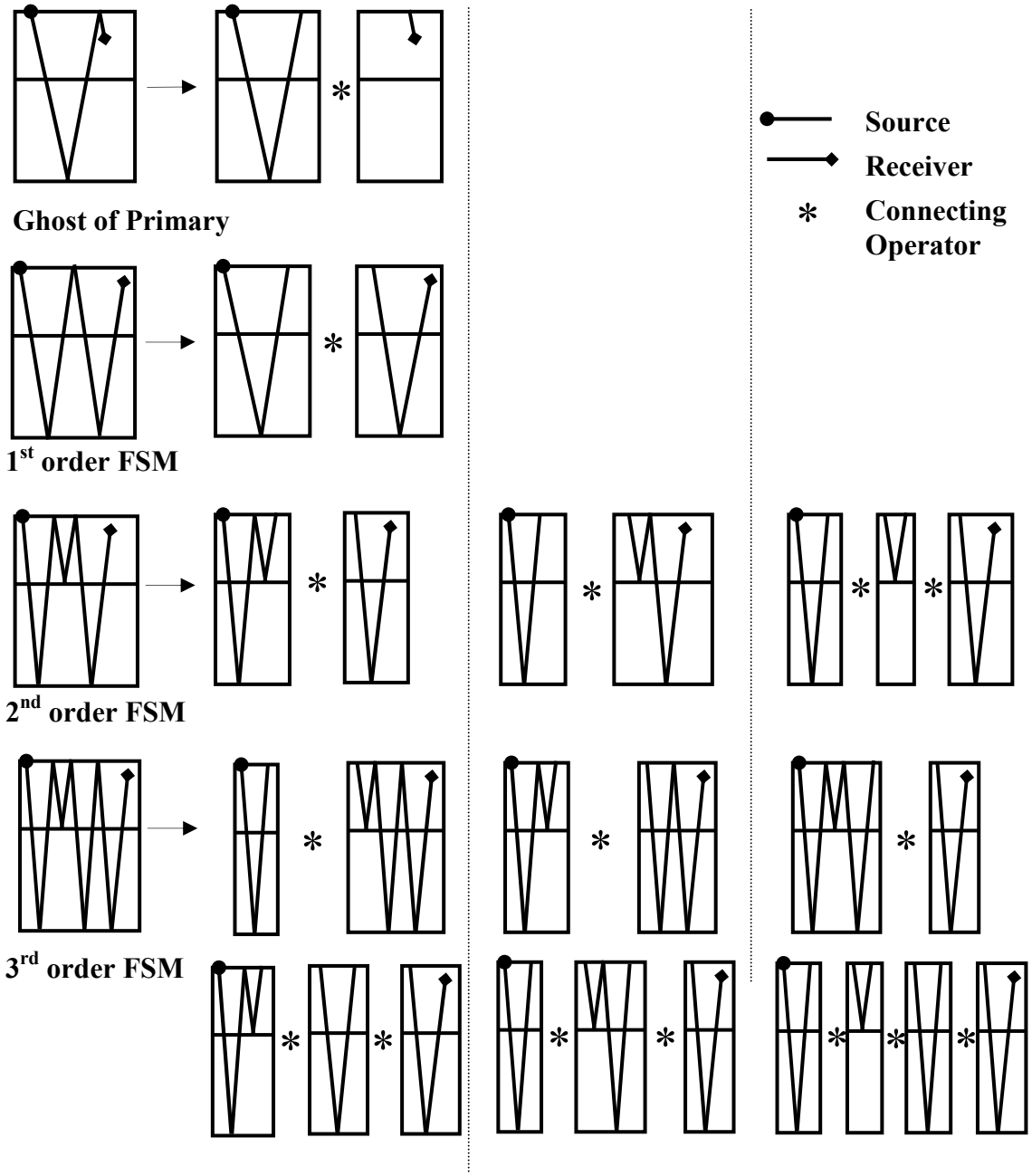

Figure A.2: Illustration of construction of free-surface multiples and ghosts by putting the scattering point at the free surface. In this example I have shown the case for towed-streamer data. Note that the 1st order FSM can be constructed in one way only, the 2nd order FSM can be constructed in two ways using one scattering point and in one way using two scattering points and the 3rd order FSM in three ways using one scattering point, in three ways using two scattering points and in one way using three scattering points.

APPENDIX B

ESTIMATION OF INVERSE SOURCE SIGNATURE

For the application of the Kirchhoff series described in Chapter I we require the knowledge of the "inverse source signature" a(ω). Although the source signature can be measured directly from the data, it requires special data-acquisition geometries such as vertical source, dual streamer, etc. Another way is to estimate the inverse source signature from the data, which will allow us to attenuate the predicted FSM from the data.

We need to calibrate the field data containing FSM and field of predicted FSM, so that the FSM in the two fields can be adjusted in amplitude and phase for an effective subtraction of predicted FSM from the field data. This calibration can be done by inverse source a(ω). However the calibration is complicated as the predicted FSM are spread over several fields ($\Phi_1, \Phi_2, \Phi_3 \ldots$). To effectively estimate a(ω) we must identify a portion of data where there is maximum correlation between FSM contained in raw data and the predicted FSM. To optimize the computations, it is also desired that this portion of data contain the predicted FSM defined by only one of the above-mentioned fields. One possible portion of data defined only by one field is the portion of predicted FSM above the second-order FSM of the sea-floor reflection (Ikelle et al. 1997).

Let us look at the mathematical translation of this selection of the portion of data.

$$\Phi_P(x_r,\omega,x_s) = \Phi_0(x_r,\omega,x_s) + a(\omega)\,\Phi_1(x_r,\omega,x_s) \quad \text{(B1)}$$

Multiplying the above equation by Φ_1^*, the complex conjugate of Φ_1, we get:

$$\Phi_1^*(x_r,\omega,x_s)\Phi_P(x_r,\omega,x_s) = \Phi_1^*(x_r,\omega,x_s)\Phi_0(x_r,\omega,x_s) + a(\omega)\Phi_1^*(x_r,\omega,x_s)\Phi_1(x_r,\omega,x_s) \quad \text{(B2)}$$

where * denotes a complex conjugate.

From the previous discussion we know that Φ_P contains primaries only, Φ_0 is raw data and Φ_1 is field of predicted multiples. Assuming that there is no correlation between primaries and first order multiples in the portion of data under consideration, (B2) becomes

$$0 = \Phi_1^*(x_r,\omega,x_s)\Phi_0(x_r,\omega,x_s) + a(\omega)\Phi_1^*(x_r,\omega,x_s)\Phi_1(x_r,\omega,x_s) \quad \text{(B3)}$$

Thus, we can estimate the inverse source signature using least square criterion as follows:

$$a(\omega) = \frac{\int dx_r \int dx_s N(x_r,\omega,x_s)}{\varepsilon^2 + \int dx_r \int dx_s Q(x_r,\omega,x_s)} \quad \text{(B4)}$$

where

$$N(x_r,\omega,x_s) = \Phi_1^*(x_r,\omega,x_s)\Phi_0(x_r,\omega,x_s)$$

and

$$Q(x_r,\omega,x_s) = \Phi_1^*(x_r,\omega,x_s)\Phi_1(x_r,\omega,x_s)$$

We notice that $N(x_r, \omega, x_s)$ is the cross correlation of the data, $\Phi_0(x_r,\omega,x_s)$, and the predicted FSM, $\Phi_1(x_r,\omega,x_s)$, in the portion of the data located above the second order water bottom multiple, while $Q(x_r, \omega, x_s)$ is the autocorrelation of the predicted first order FSM in the same portion of data.

ε^2 is a relatively small constant introduced to ensure the numerical stability for of the estimation of $a(\omega)$.

Since we are assuming no correlation between primary and FSM, we have to limit our cross-correlation window to around zero lag so that we capture the cross-correlation between the first-order water-bottom multiple of raw data and the first-order water-bottom multiple of the predicted data. The time lag for cross correlation between the primary of the water bottom and the predicted first water-bottom multiple and cross correlation between first order FSM and the predicted first order FSM will correspond the two-way travel time in the water column. Since we are assuming deep-sea exploration, the two events are easily separable. Also the autocorrelation window should also be chosen around zero-lag to eliminate any noise due to correlation at different time lags.

VITA

Name: Shantanu Kumar Singh

Address: 72-A, Badshah Bagh, Lucknow University

Lucknow, India 226007

Email Address: shanu07@yahoo.com

Education: B. Sc. (Physics, Geology), Lucknow University, Lucknow, India (1993)

M. Tech. Applied Geophysics, University of Roorkee, Roorkee India (1996)